A Hierarchical Interface-enriched Finite Element Method for the Simulation of Problems with Complex Morphologies

THESIS

Presented in Partial Fulfillment of the Requirements for the Degree Master of Science in the Graduate School of The Ohio State University

By

Jorge Luis Barrera Cruz

Graduate Program in Mechanical Engineering

The Ohio State University

2015

Master's Examination Committee:

Soheil Soghrati, Advisor

Rebecca Dupaix

Marcelo Dapino

Abstract

In the last few decades, the finite element method (FEM) has become one of the most important computational tools for the simulation of engineering problems. Due to the increasing popularity of this method, a heavy body of research has focused its attention to the development of advanced FEM-based techniques for the treatment of complex phenomena, including intricate morphologies. This thesis introduces a hierarchical interface-enriched finite element method (HIFEM) for the mesh-independent treatment of the mentioned type of problems. The HIFEM provides a general, and yet easy-to-implement algorithm for evaluating appropriate enrichment in elements cut by multiple interfaces. In the automated framework provided by this method, the construction of enrichment functions is independent of the number and sequence of the geometries introduced to nonconforming finite element meshes. Consequently, the HIFEM algorithm eliminates the need to modify/remove existing enrichment every time a new geometry is added to the domain. The proposed hierarchical enrichment technique can accurately capture gradient discontinuities along material interfaces that are in close proximity, in contact, or intersecting with one another using nonconforming finite element meshes for discretizing the problem. The main contribution of this thesis is the development and implementation of the two-dimensional higher-order HIFEM, and in particular the development of a new hierarchical enrichment scheme for six-note triangular elements. Furthermore, this manuscript presents a new enrichment scheme to

simulate strong discontinuities (cracks) in linear elastic fracture mechanics problems. Special attention is given to the available strategies to improve the level of precision and efficiency of the simulations. A detailed convergence study for the enrichment technique that yields the highest precision and the lowest computational cost is also presented. Finally, the author illustrates the application of the higher-order HIFEM for simulating the thermal and deformation responses of a variety of engineering problems with complex geometries, including porous media, fiber-reinforced composites, and quasi-static cracks in a heterogeneous domain.

Dedication

A mi familia, mis amigos y mi patria.

Por un mejor futuro para todos.

Acknowledgments

I would like to express my sincere appreciation to the many individuals who supported me in the pursuit of this degree. First, my genuine thanks and admiration to Dr. Soheil Soghrati, my advisor, who gave me the opportunity to be part of his research group. Thanks to Dr. Soghrati I could immerse myself in the field of computational mechanics over the past two years, which helped me develop key skills to build a strong foundation for meeting future academic challenges. I owe Dr. Soghrati the deepest gratitude for his continuous guidance, encouragement and patience (especially with my writing ability), without which this thesis would not have been possible. It was a great learning experience for me to have worked with him. I would also like to thank Dr. Marcelo Dapino and Dr. Rebecca Dupaix for taking time out of their busy schedules to serve on my thesis committee.

Second, I would like to thank my fellow researchers at the Automated Computational Mechanics Laboratory (ACML), Bowen Liang, Weijie Mai, Hossein Ahmadian, Ricardo Álvarez and Daniel Darvish. You kept me working hard and provided many laughs (that kept me sane) along the way. I learned a great deal from you not only from your feedback in academic endeavors, but also from a myriad of interesting topics about science, entertaining, and life in general. You have been a positive influence in my development towards reaching my personal and professional goals. More than labmates, you were my family away from home.

Third, I want to thank my family. To my mother and grandmother, Jenny and Mercy, for being in contact almost every single night since I left my home country just to know I arrived okay at my apartment after long days in the lab. To my sister, Yesenia, for taking care of everything until I come back home. And of course, to my uncle, Julio César, who has always been there for me. You all have provided me unending love and support that allowed me to keep moving forward and never give up. Although you may never read or understand the contents of this thesis, I know you are pleased to know I have reached this point in my life. I can only promise to continue my career knowing it is in loving devotion to you.

Finally, I want to thank the Secretaría de Educación Superior, Ciencia, Tecnología e Innovación (Senescyt – Ecuador) for supporting me financially throughout the process of obtaining a Master's Degree. I would not be here now writing these lines had not my home country decided to invest in their people for a better future. I will honor your trust in me by keep acquiring new knowledge and skills, and return to help build a new country after finishing my graduate education.

Vita

April 1988	Born in Guayaquil, Ecuador
2006	Graduated from Rubira High School
2011	B.S.M.E. Escuela Superior Politécnica del Litoral (ESPOL), Magna Cum Laude.
2008 to 2011	Teaching Assistant, Mechanical Engineering and Production Sciences Department, ESPOL.
2011 to 2013	Director of Operations, Jupesa: Corrosion Control.

Fields of Study

Major Field: Mechanical Engineering

Table of Contents

List of Tables

List of Figures

Chapter 1: Introduction

1.1) Background

During the past few decades, the finite element method (FEM) has become one of the top choices for the computational modeling of a variety of engineering phenomena. However, regardless of the underlying physics, generating the appropriate finite element (FE) mesh to achieve an adequate performance remains a key challenge in problems presenting complex geometries [1]. This occurs in part because of the often laborious and time consuming mesh generation process. The complexity of this process increases even further when dealing with problems with evolving morphologies such as transient phenomena and design optimization studies, which require the automated regeneration of new FE meshes or their adaptive refinement throughout the simulation [6], [7], [8]. In addition, the quality of this conforming FE mesh, i.e., its refinement level and aspect ratio of elements, has a crucial impact on the accuracy and stability of the FEM approximation [2], [3], [4], [5]. Even when employing state-of-the-art commercial software packages, creating such conforming meshes requires significant amount of human intervention, which can also lead to the creation of oversimplified models that neglect details in the geometry.

Extensive research effort has been directed to ease the aforementioned difficulties in solving problems with localized features that are not efficiently determined by mesh refinement. Alternative numerical techniques such as the boundary elements method

(BEM) [9], [10], [11], meshfree methods (MMs) [12], [13], [14], [15], and mesh-independent FEMs [16], [17], [18] have successfully been applied to a variety of engineering problems with intricate strong and weak discontinuities. One of the most popular methods in the latter category, the eXtended Finite Element Method (XFEM) [19], [20], employs the partition of unity method locally to enrich the interpolation. This method provides independence between the nonconforming mesh and the problem morphology to simulate discontinuous phenomena by incorporating a priori knowledge in the enrichment located on existing nodes. For example, in linear elastic fracture mechanics problems, discontinuous and singular functions are added to standard polynomial basis functions for nodes that belong to elements that are in close proximity to cracks to provide an accurate approximation. Contributions of the XFEM are not limited to fracture mechanics problems, though. In the literature we can find numerous applications of the XFEM to a variety of physics phenomena including contact problems, multiscale problems, and material or phase interfaces [21], [22]. The development of more accurate and robust XFEM schemes continues to be an active area of research to this day.

While XFEM achieves accurate approximations in problems with discontinuities, handling blending elements and Dirichlet boundary conditions at enriched nodes remains a challenge in the implementation of this method. An alternative mesh independent technique that obviates the above intricacies is the Interface-enriched Generalized FEM (IGFEM). This method relies on enrichment functions associated with generalized degrees of freedom (dofs) to enrich the solution field along material interfaces to simulate

the mismatch between the phases involved. The IGFEM has been applied to several multiphase problems in [24], [25], [26] and [27]. Among the advantages of this method one can cite low computational cost and, unlike XFEM, a straightforward treatment of Dirichlet boundary conditions. However, a major limitation of the IGFEM is the inability to automatically enrich nonconforming elements cut by multiple material interfaces as it requires a case-by-case modification for special cases. Since the mentioned drawback can frequently happen in domains with geometries that are in close proximity or contact, the method is arguably a good choice for computer implementation in problems with complex morphologies.

Recently, Soghrati [28] has introduced the hierarchical interface-enriched finite element method (HIFEM), a fully mesh-independent technique that completely eliminates the shortcomings of the IGFEM for modeling multiphase problems with complex geometries. The HIFEM can accurately capture field/gradient discontinuities associated with the presence of material interfaces that are in close proximity or contact, while using finite element meshes that are completely independent of the domain geometry. This is made possible through special hierarchical enrichments that can easily be formulated for nonconforming elements presenting strong and weak discontinuities. While yielding an optimal precision and convergence rate, one of the main advantages of the HIFEM is the ease of implementation and the ability to accommodate multiple material interfaces in nonconforming elements as shown in Figure 1. In the automated framework provided by HIFEM, the construction of enrichment functions is independent of the number and sequence of the geometries introduced to

nonconforming finite element meshes. Consequently, the automated framework of the HIFEM obviates the difficulties associated with the creation of a new mesh at each solution step, and the computation of the enriched solution of not only interfaces (weak), but also cracks (strong discontinuities) propagating freely through heterogeneous media.

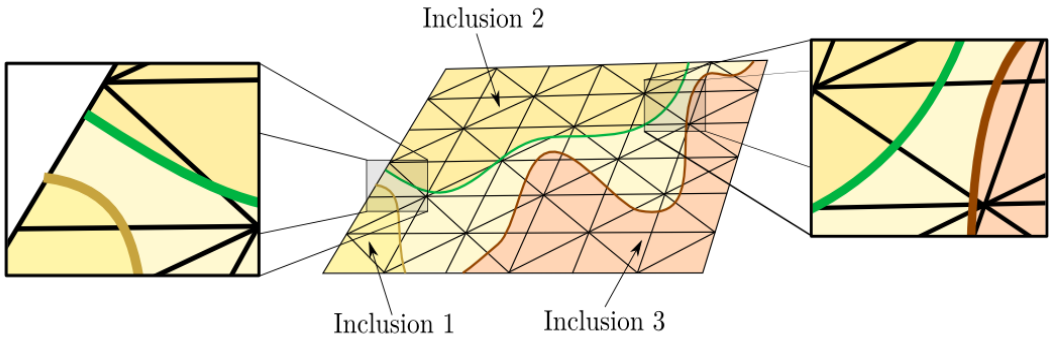

Figure 1. Example of a structured mesh containing multiple inclusions with curved geometries. The insets show material interfaces intersecting nonconforming elements that can be hierarchically accommodated by HIFEM.

Soghrati addressed details of the construction of HIFEM enrichments and their performance for problems discretized using three-node triangular FE meshes in [28]. The method was applied in heat conduction problems; however, for the simulation of stresses in structural problems, constant strain triangular (CST) elements yield a poor performance due to deficiencies such as shear locking [29]. Therefore, the use of higher-order elements is more attractive for modeling such problems.

1.2) Overview of Thesis

The objective of this thesis is to introduce a higher-order hierarchical interface-enriched finite element method (HIFEM) to obviate issues associated with creating conforming meshes for simulating problems with field and gradient discontinuities. This manuscript describes the HIFEM algorithm implementation including specifications for the construction of children elements and integration scheme. In addition, different approaches for constructing higher-order HIFEM enrichment functions associated with six-node triangular Lagrangian elements are discussed. Quadratic distorted elements are implemented after considering the advantages and drawbacks of different approaches mentioned above for constructing hierarchical enrichments. Note that although the current manuscript is particularly focused on a practical implementation of six-node triangular elements in HIFEM, the proposed algorithm can be easily expanded to other types of higher-order Lagrangian elements. To demonstrate HIFEM accuracy with respect to the standard finite element method, convergence studies are presented for multi-phase thermal and structural problems.

This thesis is structured as follows. In the following Chapter, the weak forms of the conductive heat conduction and linear elasticity problems together with an overview of the linear elastic fracture mechanics and the HIFEM formulations are presented. In Chapter 3 we briefly present different techniques for the implementation of quadratic triangular elements to the higher-order HIFEM algorithm followed by a discussion of some challenges presented. Chapter 4 reports a higher-order HIFEM convergence study of a simple heat conduction problem with straight material interfaces and a plane stress

problem with circular inclusions. In Chapter 5, several numerical simulations are provided to evince the higher-order HIFEM capabilities in applications for modeling porous materials, corrosion stress concentration in metals, reinforced fiber composites, and stationary cracks in heterogeneous media. Finally, a summary of the topics covered and directions for future work are given in Chapter 6.

Chapter 2: Governing Equations and Formulations

This chapter is devoted to the mathematical formulation of the physical phenomena corresponding to problems discussed in Chapters 4 and 5, together with a full description of the HIFEM formulation. The first part of this chapter presents the classical heat conduction and solid mechanics governing equations, including the specifications for modelling non-smooth situations associated with strong discontinuities existing in cracked domains for fracture solid mechanics problems. The next section is dedicated to fundamental aspects of the HIFEM formulation, including its roots in the Interface-enriched Generalized FEM and the description of the general implementation.

2.1) Heat Conduction Problems Governing Equations

Consider an open domain $\Omega \subset \mathbb{R}^2$ with the closure $\overline{\Omega}$ composed of m different material phases represented as non-overlapping partitions $\overline{\Omega} \cong \overline{\Omega}^h \equiv \cup_{i=1}^{m} \overline{\Omega}_i$. The domain boundary $\partial\Omega = \overline{\Omega} \backslash \Omega = \Gamma_D \cup \Gamma_N$ with outward unit normal vector $\mathbf{n}$ is divided into two distinct regions ($\Gamma_D \cap \Gamma_N = \emptyset$) corresponding to Dirichlet and Neumann boundary conditions (BCs), respectively. By decomposing the temperature field $u: \overline{\Omega} \rightarrow \mathbb{R}$ into $u = u_0 + u_d$, where $u_d: \overline{\Omega} \rightarrow \mathbb{R}$ such that $u_d|_{\Gamma_D} = \bar{u}$, and $\bar{u}: \Gamma_D \rightarrow \mathbb{R}$ is the prescribed temperature on Γ_D, the weak form of the conductive heat transfer governing equations is expressed as: Find $u_0 \in \mathcal{V} \coloneqq \{u_0: \overline{\Omega} \rightarrow \mathbb{R},\ u_0|_{\Gamma_D} = 0\}$ such that

$$\sum_{i=1}^{m} \int_{\Omega_i} \nabla(u_0 + u_d).\kappa_i \nabla v d\Omega + \int_{\Omega_i} vQd\Omega + \int_{\Omega_i} vqd\Gamma \ = 0 \quad \forall v \in \mathcal{V}, \tag{1}$$

where $\kappa_i: \overline{\Omega}_i \to \mathbb{R}^2 \mathrm{x}\ \mathbb{R}^2$ is the thermal conductivity tensor associated with the ith material phase, $Q: \Omega \to \mathbb{R}$ is the heat source, and $q: \Gamma_N \to \mathbb{R}$ is the applied heat flux. The continuity of temperature and heat flux conditions are weakly enforced along the interface between two adjacent subdomains $\overline{\Omega}_i$ and $\overline{\Omega}_j$ as follows

$$\begin{aligned} \mathrm{u}|_{\Gamma_i} - \mathrm{u}|_{\Gamma_j} &= 0 && \text{On} \quad \overline{\Omega}_i \cap \overline{\Omega}_j\ , \\ \kappa_i \nabla u.\,\mathbf{n_i} + \kappa_j \nabla u.\,\mathbf{n_j} &= 0 && \text{On} \quad \overline{\Omega}_i \cap \overline{\Omega}_j. \end{aligned} \tag{2}$$

The Galerkin approximation u_h for (1) can be evaluated by replacing $\mathcal{V}^h \subset \mathcal{V}$ with proper finite dimensional space (e.g., the space of Lagrangian shape functions in the standard FEM).

2.2) Linear Elasticity Problems Governing Equations

Similar to the heat conduction formulation, assuming $\mathrm{u} = \mathrm{u_0} + \mathrm{u_d}$ as the deformation response of a linear elastic continuum such that $\mathrm{u_d}: \overline{\Omega} \to \mathbb{R}^2$ and $\mathrm{u_d}|_{\Gamma_\mathrm{D}} = \bar{\mathrm{u}}$, the weak form of the linear elasticity governing equations can be written as: Find $\mathrm{u_0} \in \mathcal{W} \coloneqq \{\mathrm{u_0}: \overline{\Omega} \to \mathbb{R}^2,\ \mathrm{u_d}|_{\Gamma_\mathrm{D}} = 0\}$ such that

$$\sum_{\mathrm{i}=1}^{\mathrm{m}} \int_{\Omega_\mathrm{i}} \mathrm{L}(\mathrm{u_0} + \mathrm{u_d}).\,\mathbb{C}_\mathrm{i}\mathrm{L}^\mathrm{T}\mathrm{w}^\mathrm{T}\mathrm{d}\Omega + \int_{\Omega_\mathrm{i}} \mathrm{wbd}\Omega + \int_{\Omega_\mathrm{i}} \mathrm{wtd}\Gamma \ = 0 \quad \forall \mathrm{w} \in \mathcal{W} \tag{3}$$

Where $\mathbb{C}_i$ denotes the fourth-order elasticity tensor associated with the ith material phase, $b: \Omega \to \mathbb{R}^2$ is the body force, $\bar{u}: \Gamma_D \to \mathbb{R}^2$ is the prescribed displacement, $t: \Gamma_N \to \mathbb{R}^2$ is the applied traction field, and the differential operator L is given by

$$L = \begin{bmatrix} \frac{\partial}{\partial x} & 0 & \frac{\partial}{\partial x} \\ 0 & \frac{\partial}{\partial y} & \frac{\partial}{\partial y} \end{bmatrix}. \tag{4}$$

Given $E_i: \Omega_i \to \mathbb{R}$ as the as the elastic modulus, and $v_i: \Omega_i \to \mathbb{R}$ as the prescribed Poisson ratio of each material phase, the matrix form of $\mathbb{C}_i$ for a plane stress problem can be written as

$$\mathbb{C}_i = \frac{E_i}{1 - \upsilon_i^2} \begin{bmatrix} 1 & \upsilon_i & 0 \\ \upsilon_i & 1 & 0 \\ 0 & 0 & \frac{1 - \upsilon_i}{2} \end{bmatrix} \tag{5}$$

The continuity of displacements and tractions along the interface between adjacent subdomains $\bar{\Omega}_i$ and $\bar{\Omega}_j$ is given by

$$\begin{aligned} u|_{\Gamma_i} - u|_{\Gamma_j} &= 0 && \text{On} \quad \bar{\Omega}_i \cap \bar{\Omega}_j\ , \\ \mathbb{C}_i L^T u^T . \mathbf{n_i} + \mathbb{C}_j L^T u^T . \mathbf{n_j} &= 0 && \text{On} \quad \bar{\Omega}_i \cap \bar{\Omega}_j . \end{aligned} \tag{6}$$

The Galerkin approximation u_h for (3) can be evaluated by replacing $\mathcal{W}^h \subset \mathcal{W}$ with proper finite dimensional space.

Fracture mechanics problem formulation

Consider a cracked domain Ω following the same governing equations described above for structural problems. A crack is denoted by Γ_C such that Γ_D, Γ_N and Γ_C are

partitions of $\partial\Omega$; and that Γ_D and Γ_N are on the boundary of the non-cracked domain $\bar{\Omega}$. Assuming a traction free condition on the crack, equation (3) is used with the following modification in the definition of the space of the admissible displacement: $\mathcal{W} = \{w \in \mathcal{V} : \mathrm{w} = \bar{\mathrm{u}} = \text{on } \Gamma_u, \mathrm{w} \text{ discontinuous on } \Gamma_C\}$.

In Williams' asymptotic displacement [31], $\mathrm{u} = u_d\ (d = 1, 2)$ in the neighborhood of the tip in polar coordinates is given by

$$u_d(r, \theta) = a_k + b_k(\theta) r^{1/2} + c_k(\theta) r + d_k(\theta) r^{3/2} + \cdots, \qquad (7)$$

where r is the distance to the tip, and θ is the angle formed between the slope of the crack at the tip and r. Note that strains and stresses components derived from equation (7) will have a component as a function of $r^{-1/2}$, which results in a singularity when $r = 0$.

2.3) HIFEM Formulation

In this section, we first review the standard FEM, GFEM, XFEM, and IGFEM formulations followed by the formulation and implementation of the HIFEM.

FEM and GFEM formulations

A given problem can be modeled using the standard FEM by discretizing the domain into m finite elements and employing a set of n shape functions $N_i(\mathbf{x})$ for approximating the field in each element, as described by the following expression:

$$u^h(\mathbf{x}) = \sum_{i=1}^{n} N_i(\mathbf{x}) u_i \tag{8}$$

The above equation cannot accurately capture gradient discontinuities unless the elements of the FE mesh conform to those geometries. If nonconforming meshes are to be used instead, the simulations can be performed using the generalized FEM (GFEM) framework [32]. In this method, a set of local enrichment functions are multiplied by the standard Lagrangian shape functions to provide a sparse linear system of equations. In the GFEM approximation given by

$$u^h(\mathbf{x}) = \sum_{i=1}^{n} N_i(\mathbf{x}) \tilde{u}_i + \sum_{i=1}^{n} N_i(\mathbf{x}) \sum_{j=1}^{n_{en}} \varphi_{ij}(\mathbf{x}) \hat{u}_{ij}, \tag{9}$$

the variable $\tilde{u}_i$ does not necessarily approximate the field at node i since the contribution of the second term has to be taken into account in enriched regions of the domain.

Despite the simplicity of the formulation, some implementation issues need to be addressed in the GFEM. In (9), a prescribed value of the solution field cannot be assigned to enriched nodes in a boundary with essential condition. Hence, to enforce Dirichlet boundary conditions, Lagrange multipliers or the penalty method might be required. In addition, the existence of incomplete terms of the enrichment in cases where only some of the nodes are enriched (e.g., in blending elements) compromises the accuracy and rate of convergence. Furthermore, in order to achieve a good accuracy, the GFEM employs integration schemes such as subdividing the enriched elements into subdomains and integrating over the resulting sub-elements. To apply the mentioned approach, the sub-

element must be created in a way such that their edges are aligned with the geometry of the discontinuities while maintaining the aspect ratio within a desired range.

The IGFEM formulation

The IGFEM formulation extends the GFEM to

$$u^h(\mathbf{x}) = \sum_{i=1}^{n} N_i u_i + \sum_{j=1}^{n_{en}} s_j \psi_j \alpha_j, \tag{10}$$

where the first term corresponds to the FEM portion of the approximation. In the second term, the coefficients s_j are scaling factors introduced to guarantee a well-conditioned stiffness matrix, ψ_j are the enrichment functions, and α_j are the generalized dofs. The main difference between equations (9) and (10) is the approach for assembling the generalized dofs. The IGFEM no longer uses the concept of partition of unity, but achieves a unified enrichment by sharing the same generalized dofs between enriched nodes of adjacent elements [23]. These enrichment functions vanish at the location of the nodes of the nonconforming mesh; hence, the approximations u_i directly yield the solution field at the location of the nodes of the original mesh. Note that the enrichment holds no physical meaning, but represents the magnitude of departure from the root solution of the nonconforming mesh.

Implementing the IGFEM for simulating problems with highly complex and heterogeneous domains is a challenging task. Several cases must be considered for discretizing nonconforming elements by multiple materials interfaces. Although the development of an algorithm to systematically handle all possible cases is feasible, this

approach is no longer practical since it involves the tedious labor of adding the special cases one by one. Furthermore, the sequence of the material interfaces added to the problem can also be an issue since the IGFEM removes existing sub-elements and redefines the discretized parent element for each interface cutting the background mesh.

The HIFEM formulation

The HIFEM overcomes the IGFEM limitation associated with constructing enrichment functions in elements cut by multiple interfaces via a recursive algorithm for evaluating the enrichment functions [28]. The HIFEM approximation of the field u^h for a domain $\Omega \cong \Omega^h$ discretized into M nonconforming elements can be written as

$$u^h(\mathbf{x}) = \sum_{i=1}^{n} N_i^p u_i + \sum_{j=1}^{n_{en}} s_j^{(h)} \psi_j^{(h)} \alpha_j^{(h)}, \tag{11}$$

where the first term of the right hand side is associated with the standard FEM formulation, and the second terms represents the degrees of freedom corresponding to the enrichment for the strong and weak discontinuities. In (11), u_i represents the value of the variable to be solve for at the ith node of the nonconforming element; $\alpha_j^{(h)}$ is the generalized degree of freedom corresponding to the jth node created at the intersection of the hth material interface with the element edges; $\{N_i^p\}_{i=1}^{n}$ and $\left\{\psi_j^{(h)}\right\}_{j=1}^{n_{en}}$ are sets of n Lagrangian shape functions and n_{en} hierarchical enrichment functions at the hth hierarchical level, respectively; and $s_j^{(h)}$ is a scaling factor applied to the enrichment to avoid an ill-conditioned stiffness matrix due to bad aspect ratios of sub-elements. For

higher-order elements the general formulation need not be modified since the underlying concepts of the method remains the same. The details of the computation of the scaling factor will be revisited in the next section.

The HIFEM enrichments attached to the generalized degrees of freedom are hierarchically introduced to the approximate field in the regions where material interfaces cut the edges of the nonconforming mesh. Figure 2 shows a simple scheme that illustrates the construction of these enrichments to a single three-node triangular element cut by two interfaces. For each cut, we discretize the affected area into smaller triangular (*children*) elements that conform to each material interface. As seen in Figures 2b and 2c, these children elements will then serve as *parent* elements for the next material interface following the same hierarchical discretization scheme until all interfaces cutting the original parent element (*root* element) are handled. The order in which the multiple material interfaces are processed does not affect the HIFEM accuracy.

The computation of enrichment functions associated with the jth interface node at the hth level of hierarchy of n_{hl} hierarchical levels is given by

$$\psi_{total} = \sum_{h=1}^{n_{hl}} \psi^h = \sum_{h=1}^{n_{hl}} \sum_{j=1}^{n_{in}^{(h)}} \sum_{k=1}^{n_c^{(h)}} N_r^k, \tag{12}$$

where $n_{in}^{(h)}$ is the number of interface nodes at the hth level of hierarchy, $n_c^{(h)}$ is the number of children elements connected to the jth interface node at this level, and N_r^k is the rth Lagrangian shape function of the kth child element.

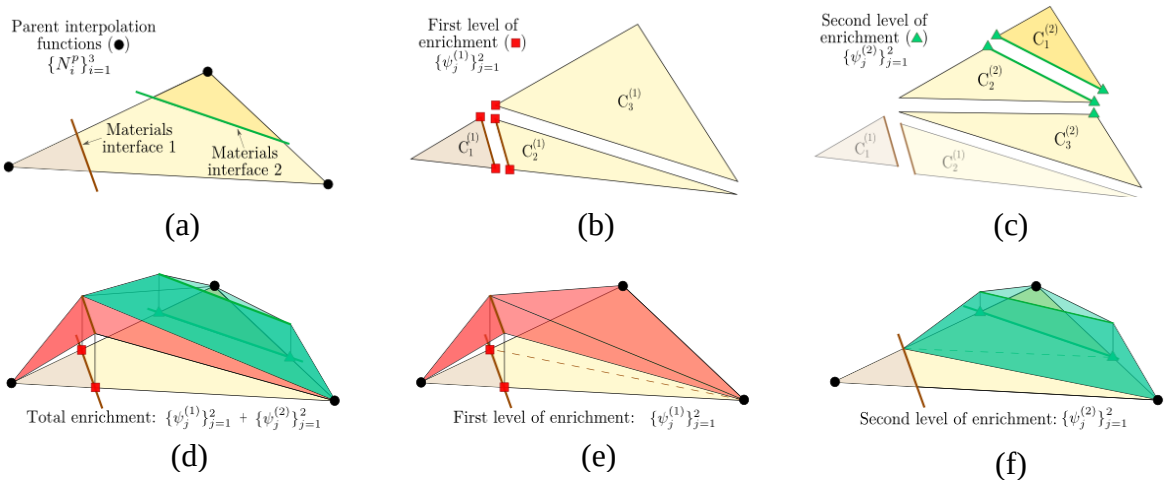

Figure 2. Process of creating HIFEM children elements in nonconforming three-node triangular element: (a) root element cut by two material interfaces; (b) children elements and interface nodes created at the first level of hierarchy; (c) children elements and interface nodes created at the second level of hierarchy from the intersection between material interface 2 and child element $C_3^{(1)}$ of the first level of enrichment; (d, e, f) enrichment functions belonging to the total enrichment (a), the first level of hierarchy (b), and the second level of hierarchy (c), respectively.

As depicted in Figure 2, the construction of children elements is straightforward for linear enrichment. Enriched nodes are placed at the intersection points of each interface with the elements constructed at the highest level of hierarchy. However, for higher-order elements, more than one configuration of the HIFEM enrichment can be adopted. In order to implement the optimal approach, next chapter is devoted to the analysis of different configurations of quadratic enrichment.

Scaling factor

Ill-conditioning of the stiffness matrix can affect the performance of iterative linear solvers, or interfere with the convergence of solvers for nonlinear problems. In the

standard FEM, special consideration must be given to children elements with high aspect ratios since these elements deteriorate the conditioning of the stiffness matrix. The HIFEM obviates the issue of monitoring the quality of the children elements constructed for enrichment by employing a simple and efficient scaling factor $s_j^{(h)}$ (see equation (11)) based on the geometrical features of the element and the location of the enriched node being scaled with respect to the nodes in its neighborhood. As a consequence, children elements can have any type of size and shape configurations without compromising the conditioning of the system.

The enrichment function associated with the jth enriched node of a child element created at the hth hierarchical level is scaled down by using the following expression:

$$s_j^{(h)} = \frac{\min(\|\mathrm{x}_1 - \mathrm{x}_{int}\|, \|\mathrm{x}_2 - \mathrm{x}_{int}\|, \|\mathrm{x}_3 - \mathrm{x}_{int}\|)}{l_p} \sqrt{\frac{J_p}{J_c}}, \tag{13}$$

where x_1 and x_2 are the adjacent nodes located over the intersecting edge, x_{int} is the intersection point over the edge, x_3 is a point over the opposite edge perpendicular to x_{int}, l_p represents the length of the parent element, and J_p and J_c correspond to the determinant of the Jacobians of the parent and child elements containing the node located at x_{int}, respectively.

The scaling factor is employed to mitigate the effect of either large gradients of the Lagrangian enrichment functions, or extremely small determinants of the child element Jacobian. The former is a result of children nodes located extremely close to an adjacent node or an element edge, while the latter occurs when the size of a child element

associated with the enriched node is extremely small in comparison with the corresponding parent. Both situations are shown in Figure 3.

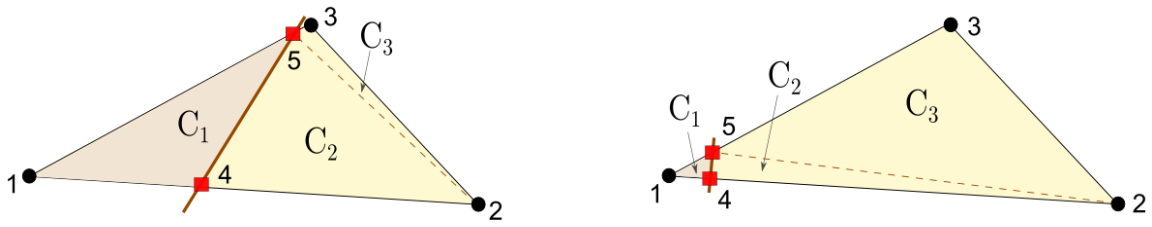

(a) (b)

Figure 3. Examples of children elements that could deteriorate the conditioning of the system of equations in absence of a proper scaling factor. In (a), the conditioning can be affected by the small relative distance between enriched node 5 and parent node 3. In (b), the small area of C_1 can also influence the condition number.

Note that not all the enriched nodes need to be scaled, but only those below a given threshold defined in the algorithm. Furthermore, scaling factors are used in the computation of element stiffness matrices. Thus, unlike most of the strategies introduced for improving the conditioning of other mesh-independent methods (e.g., preconditioners in XFEM [33], [34]), no additional computation/modification is needed for the global stiffness matrix.

Numerical Integration

For the numerical integration, the HIFEM uses a recursive framework to evaluate the smallest children elements (e.g., the ones located at the highest level of hierarchy) contained in each root element together with the corresponding portion of the parent elements of subsequent hierarchical levels. The algorithm computes the enrichment for

interface nodes at each level, choosing material properties assigned to the highest level of hierarchy.

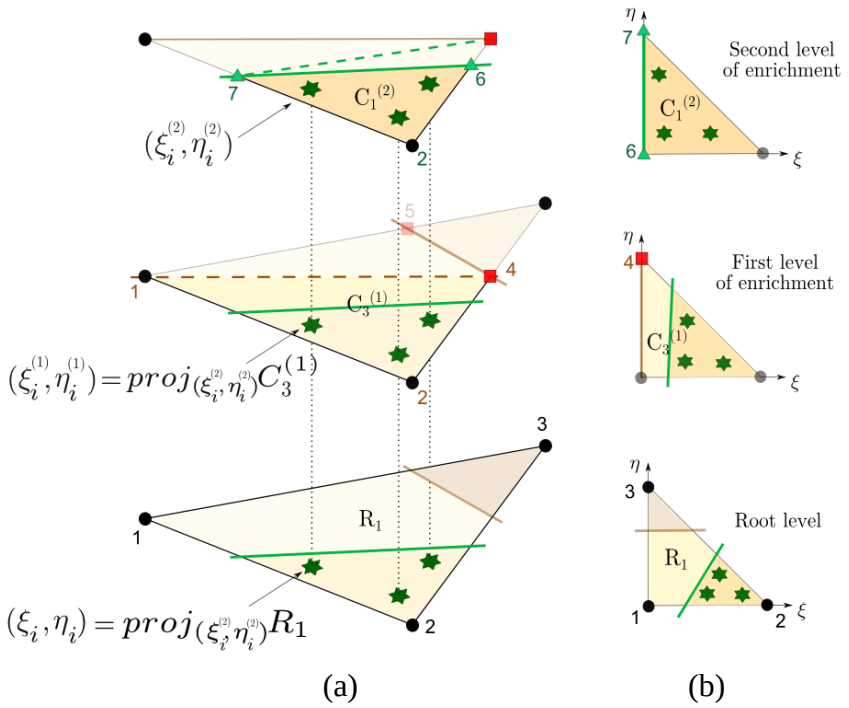

Figure 4. Integration process of a three-point quadrature rule over a triangle. (a) Gauss points $\left(\xi_i^{(2)}, \eta_i^{(2)}\right)$ are integrated simultaneously on child element $C_1^{(2)}$, and portions of elements $C_3^{(1)}$ and R_1. (b) Location of the mapped gauss points $\left(\xi_i^{(2)}, \eta_i^{(2)}\right)$ in the isoparametric domains of elements $C_1^{(1)}$and R_1.

Figure 4 illustrates how HIFEM enrichment functions are integrated simultaneously at all levels of hierarchy. In this example, the algorithm integrates element $C_1^{(2)}$, together with the portions of elements $C_3^{(1)}$ and R_1 corresponding to the area of $C_1^{(2)}$. Each quadrature point $(\xi_i^{(2)}, \eta_i^{(2)})$ is mapped from the global coordinates system to the corresponding local coordinates system so that $(\xi_i^{(1)}, \eta_i^{(1)})$ and (ξ_i, η_i)

integrate smaller portions of the isoparametric reference triangle. Since enriched nodes are evaluated at the level they were created, only nodes 6 and 7, and node 4 are evaluated at the second and first level of enrichment, respectively. Note that all nodes corresponding to the root element are always evaluated at the root level. After repeating this integration scheme for all elements at the highest level of hierarchy, the elements contained in lower levels will also be integrated. Figure 5 presents the flow chart associated with this algorithm.

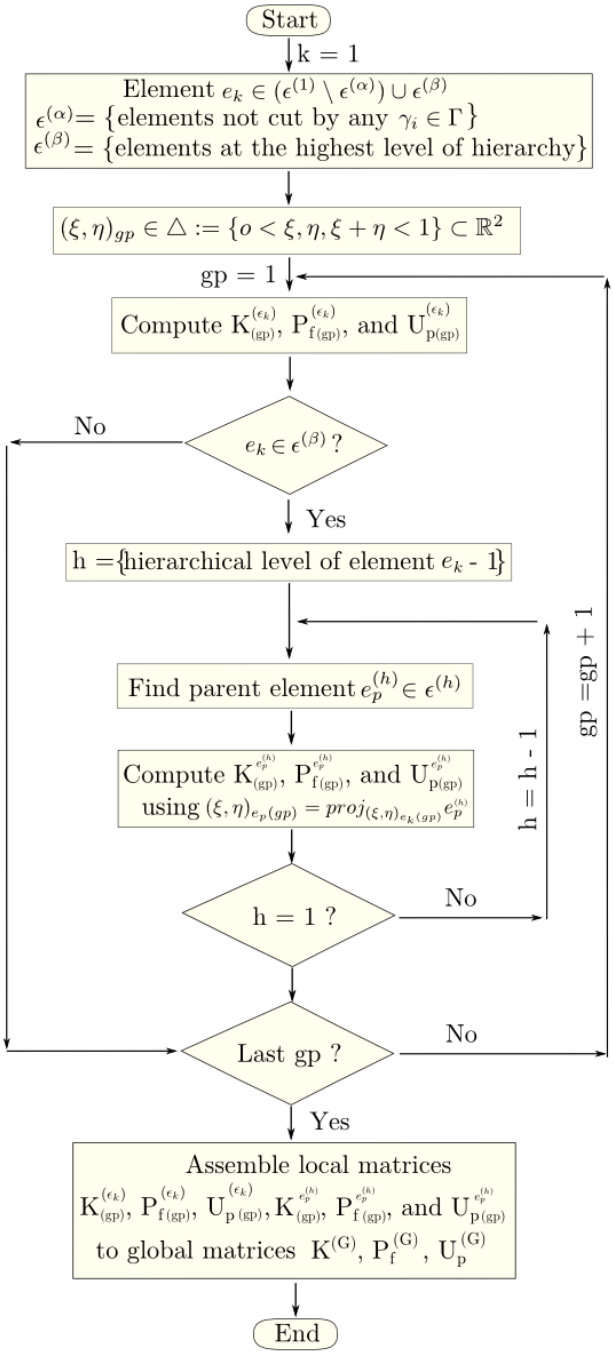

Figure 5. Simple flow chart that describes the process of hierarchical integration of parent and children elements simultaneously.

Basic HIFEM algorithm

Figures 6 shows the process of creating hierarchical enrichments in the HIFEM.

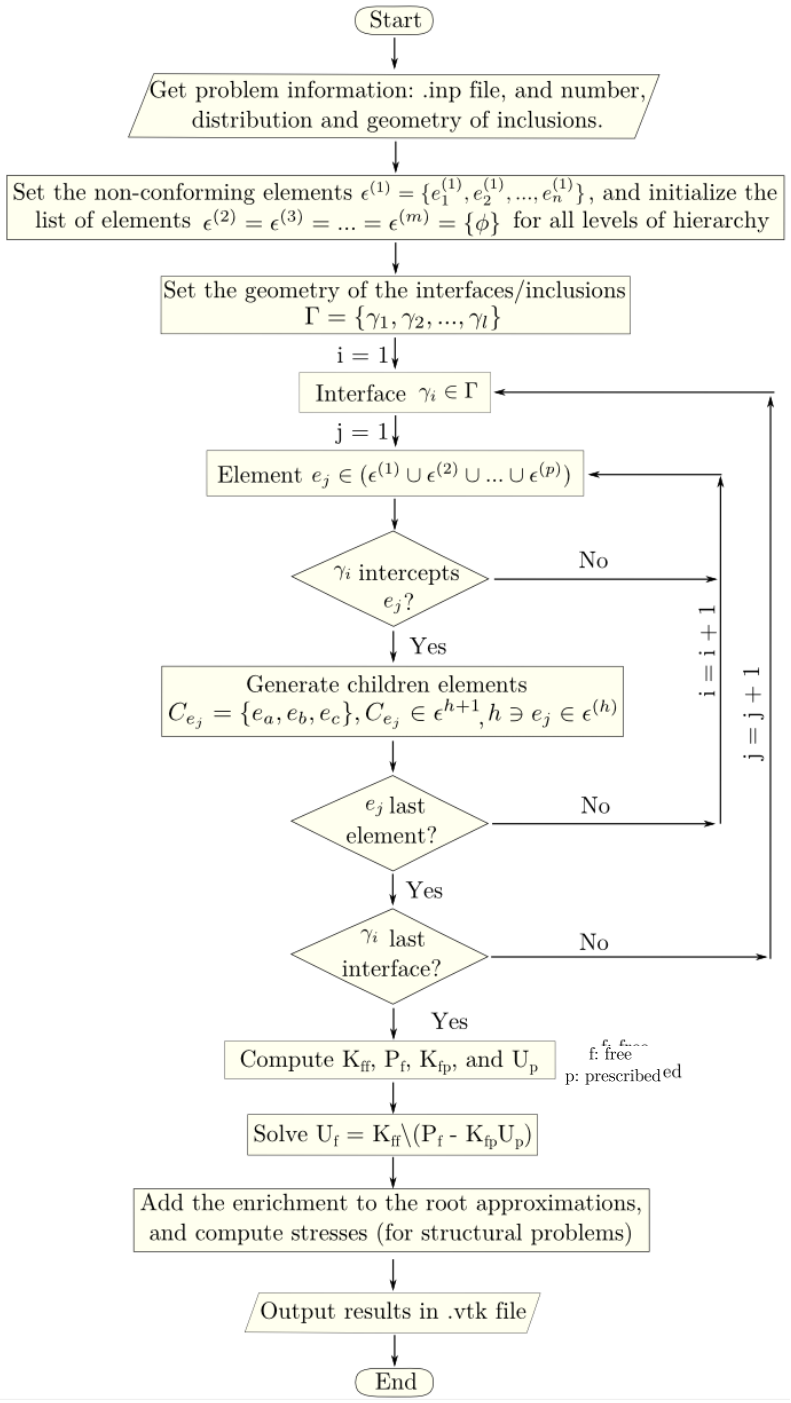

Figure 6. Simple flow chart for the HIFEM algorithm.

Chapter 3: Higher-order HIFEM Algorithm

While the recursive algorithm described in the previous section remains unchanged for the higher-order formulation, the construction of the children elements must be studied in more detail. Linear elements cannot be used for enrichment when the approximation of the root solution is described by a quadratic field since they fail the reconstruction of a linear field with gradient discontinuities. Higher order polynomial terms of order n_r in the Lagrangian shape functions of the root elements can only be eliminated by enrichment constructed by shape functions of order n_e, with $n_e \geq n_r$. For example, if the HIFEM algorithm receives a nonconforming quadratic FE mesh as input to solve a given problem, the enrichment functions should be at least second order polynomial basis functions.

3.1) 1D Higher-order HIFEM

To illustrate the aforementioned concept, consider the one-dimensional steady-state heat conduction problem shown in Figure 7. In this example, one quadratic element mesh simulates a domain consisting of three infinite plane homogeneous walls with different thicknesses and thermal conductivities, no heat generation, and boundary conditions of temperature u_0 and heat flux q_0. The HIFEM algorithm identifies the three-node element as a root element and creates quadratic enrichment about each interface in subsequent levels as follows. Children elements $C_1^{(1)}$ and $C_2^{(1)}$, together with enriched

nodes 4 and 5, are constructed in the first level of enrichment from the intersection of Interface 1 with the root/parent element. Similarly, children elements $C_1^{(2)}$and $C_2^{(2)}$, and enriched nodes 6 and 7, are generated in the second level of enrichment from the intersection of Interface 2 with element $C_1^{(1)}$, which is now acting as parent element. The combined solution is obtained by adding the higher-order enriched nodes solutions (nodes 4, 5, 6 and 7) to the interpolated value of the field of the root solution (nodes 1, 2 and 3) at the location of the corresponding nodes. As mentioned earlier, this approach passes the patch test using quadratic functions for both root and enrichment portions of the solution.

The piecewise linear thermal response is captured by the HIFEM approximation since the quadratic term x^2 in the Lagrangian shape functions of the root element is eliminated by similar terms in the enrichment functions. Figure 8 shows the resulting hierarchical structure for this simple example. Note that children elements $C_1^{(2)}$ and $C_2^{(2)}$ utilize nodes 2 and 5, respectively, instead of defining new enriched nodes at the midpoints of their edges. This results in a distorted configuration. A detailed explanation of the reasons for using this configuration is provided in the next section.

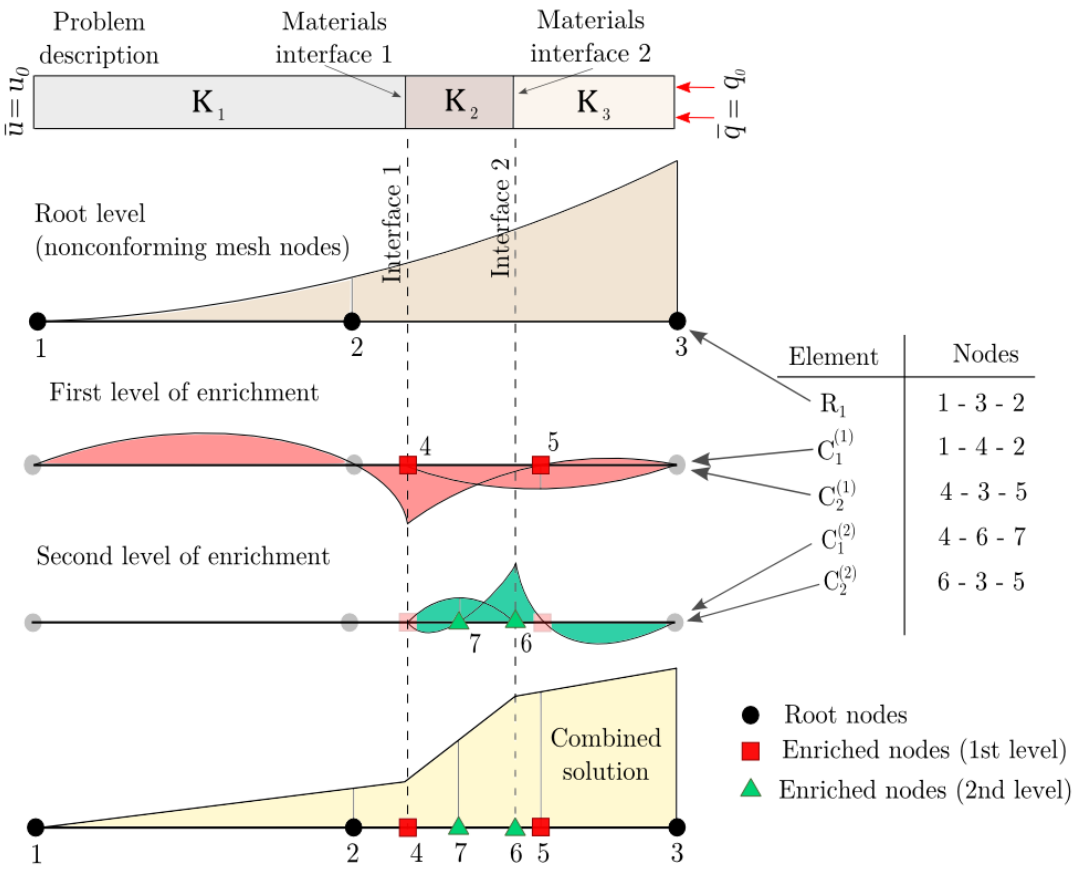

Figure 7. A three-phase one-dimensional heat conduction problem. The root element is enriched by children elements constructed sequentially from the intersection of each interface with the discretized domain. The combined solution is calculated adding the enrichment to the root solution.

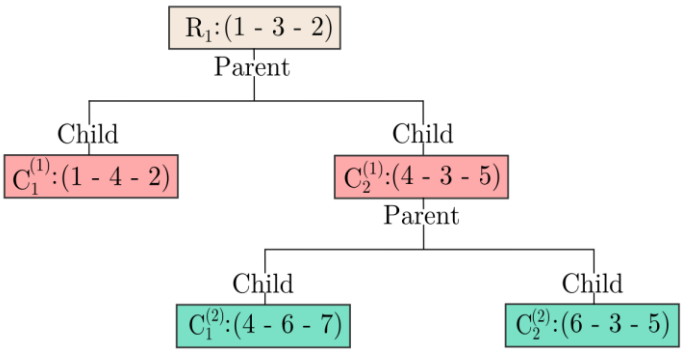

Figure 8. Hierarchical structure of the children elements constructed for the example problem presented in Figure 7.

3.2) 2D Higher-order HIFEM

In a two-dimensional domain, the HIFEM algorithm follows a similar procedure to the one described above. For nonconforming meshes consisting of six-node triangular elements, we must implement the same type of element (six-node triangular elements) as children elements to compute the enrichment. Different Lagrangian shape functions for enrichment cannot be used (e.g., three-node triangular or transition elements), since they fail to reconstruct a linear field with gradient discontinuities and hence, do not pass the patch test. Although this manuscript is focused on the implementation of six-node triangular elements in HIFEM, the proposed algorithm can be expanded to other types of higher-order Lagrangian elements.

Two different schemes for constructing quadratic children elements from elements cut by a material interface are presented in Figure 9. In the first approach shown in Figure 9a, we require a total of 8 enriched nodes to create the children elements since the midpoint parent nodes 4 and 6 on the edges cut by the interface are not included. This approach results in the formation of a singular global stiffness matrix due to redundant enriched degrees of freedom. In order to eliminate this issue, one can enforce the enrichment approximation to be zero at the location of the parent nodes. Nevertheless, this approach creates two additional degrees of freedom and the enrichment needs to be constrained with respect to the location of the corresponding parent mid-side nodes.

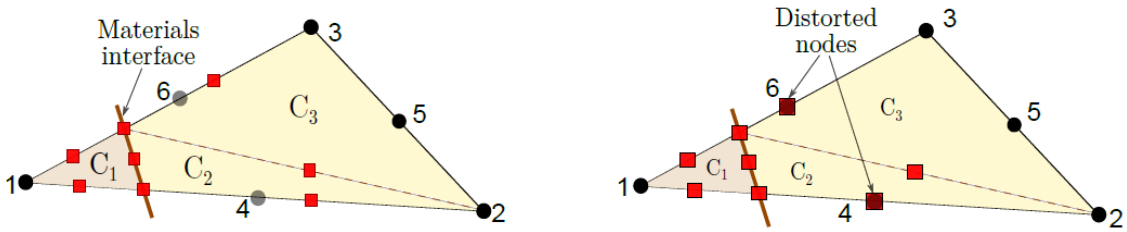

(a) (b)

Figure 9. Two approaches for constructing children elements in a six-node triangular nonconforming element cut by a single interface. In the approach shown in (a), nodes 4 and 6 of the parent element are not considered in the construction of the children elements. Conversely, in the approach in (b), all parent nodes are also part of the enrichment.

An additional alternative to avoid a singular stiffness matrix can be seen in Figure 9b, where all parent nodes are included in the next hierarchical level as part of the children elements. However, even in parent elements with straight edges and straight material interfaces, this approach yields distorted children elements with non-constant Jacobians in an isoparametric formulation because such non-corner nodes of the children elements are not located in the middle of its edges. Since the HIFEM allows the material interfaces to cut the edges at arbitrary locations, the element distortion can be severe when the intersection point is close to a parent node. As a possible consequence, the use of distorted elements can have serious drawbacks in terms of computational cost and accuracy. More integration points are needed to perform accurate quadrature in distorted elements [30]. Furthermore, to compute the non-constant Jacobian of distorted children elements, a nonlinear problem must be iteratively solved at each quadrature point to map them to the local coordinates of its corresponding quadrature point in the parent element [28].

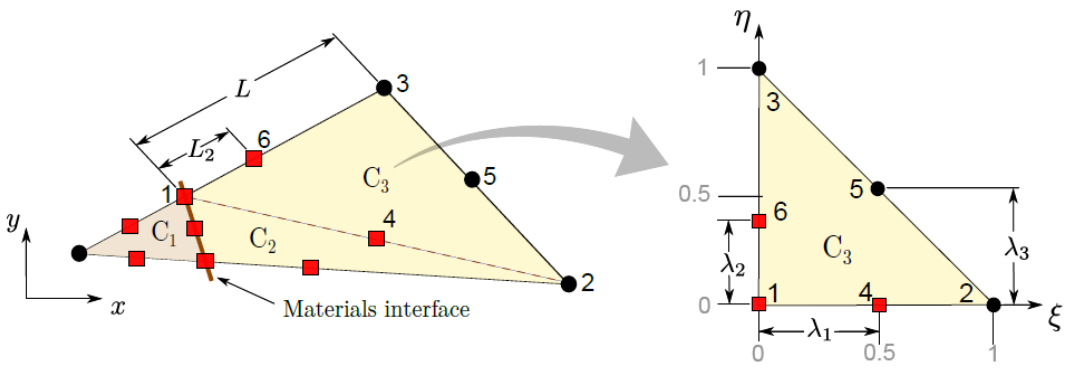

Figure 10. Mapping of a six-node triangular child element to the reference coordinates system. Parameteres λ_1, λ_2, and λ_3 represent the ratios of the distance between the non-corner and corner nodes to the length of their corresponding edges of the child element.

In order to eliminate the difficulties associated with the use of distorted children elements in the higher-order HIFEM, a third approach shown in Figure 10 is proposed. Here, the isoparametric mapping is no longer used as reference element of distorted children elements in the local coordinates system. In its place, the HIFEM algorithm employs a geometrical mapping that preserves the relative location of the non-corner nodes for both the local and global coordinates systems. The dimensionless parameters λ_1, λ_2, and λ_3 are defined from the ratio of the relative distance of a non-corner node to the length of the edge. For example, in Figure 10, the relation $\lambda_2 = \frac{L_2}{L}$ is kept in both the local and global coordinate systems. Thus, the six-node quadratic shape functions used for enrichment are not only functions of the local coordinates ξ and η, but also functions of scalar values λ_1, λ_2, and λ_3, as described in the set of equations listed in Table 1. The benefit of using the proposed mapping is that it yields a constant Jacobians for problems using distorted elements for the enrichment.

Quadratic shape functions for enrichment	
N_1	$\frac{(\xi+\eta-1)(\lambda_2\xi-\lambda_1\lambda_2+\lambda_1\eta)}{\lambda_1\lambda_2}$
N_2	$\frac{-\xi(\lambda_3\xi-\lambda_1\lambda_3-\eta+\lambda_1\eta+\lambda_3\xi)}{\lambda_3(\lambda_1-1)}$
N_3	$\frac{\eta(\lambda_2-\eta)}{(\lambda_2-1)}+\frac{\xi\eta(\lambda_2-\lambda_3)}{(\lambda_2-1)(\lambda_3-1)}$
N_4	$\frac{\xi(\xi+\eta-1)}{\lambda_1(\lambda_1-1)}$
N_5	$\frac{-\xi\eta}{\lambda_3(\lambda_3-1)}$
N_6	$\frac{\eta(\xi+\eta-1)}{\lambda_2(\lambda_2-1)}$

Table 1. Parametric quadratic shape functions for six-node triangular elements used for enrichment.

When creating children elements with straight edges, the proposed mapping yields distorted children elements with constant Jacobians. Otherwise, the distortion of children elements is minimal, and only as a result of the curvature of the interface rather than inappropriate locations of their midpoints. Note that the parametric shape functions given in Table 1 can also be utilized in the global coordinates system. However, this representation in the local coordinates system can be more beneficial since it reduces the computational cost associated with constructing enrichment functions, and facilitates the numerical integration by using local quadrature points.

3.2.1) Enrichment for Weak Discontinuities

Although the triangulation is not unique, this code follows the schemes shown in Figures 11 and 12 for the construction of enrichment for weak discontinuities. If a child node coincides with one of the parent nodes, no enrichment is attached to that node since that intersected node already yields the value of the field.

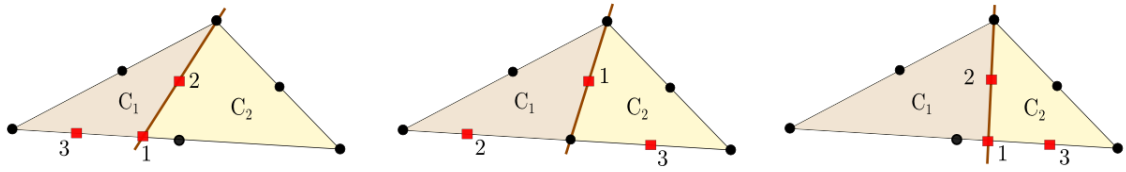

Figure 11: Configurations of enrichment for weak discontinuities cutting elements on a corner node and an edge. Two children elements and three enriched nodes are generated in all three cases.

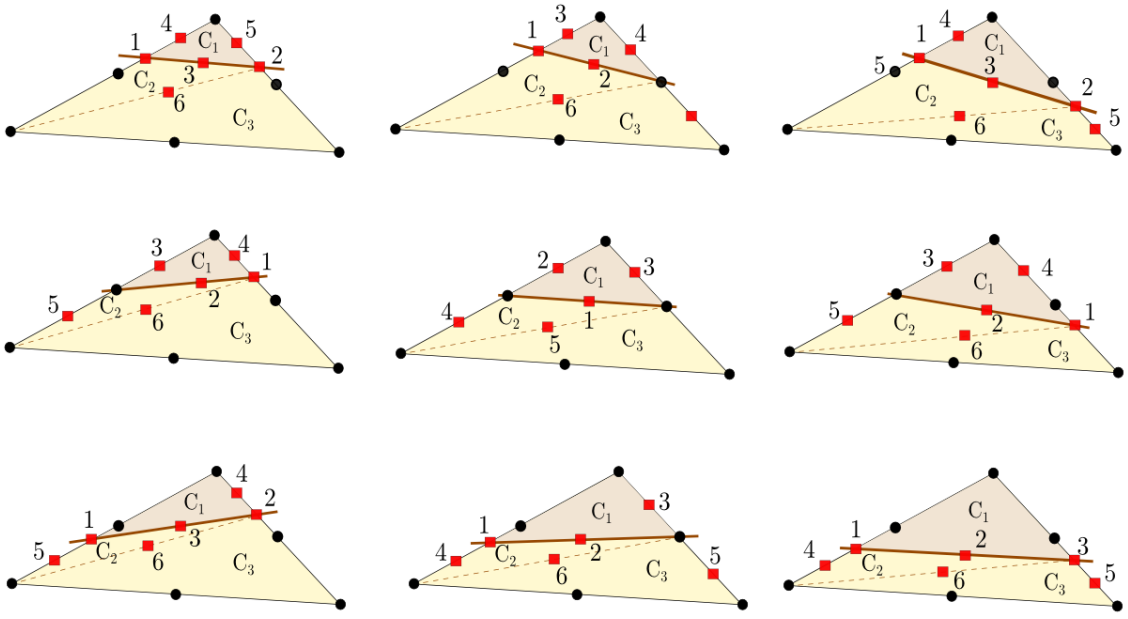

Figure 12: Configurations of enrichment for weak discontinuities cutting elements on two of its edges. Three children elements and up to six enriched nodes are generated.

Using a similar mapping scheme as the one described at the beginning of this section for the one-dimensional example, we can hierarchically create higher-order (quadratic) distorted children elements as shown in Figure 13. Interfaces can cut a triangular element into either two triangular children elements, or one triangular and one quadrilateral sub-element. For the former case, the HIFEM algorithm decomposes further the quadrilateral sub-element to have only triangular children elements following one of the configurations shown in Figures 11 and 12.

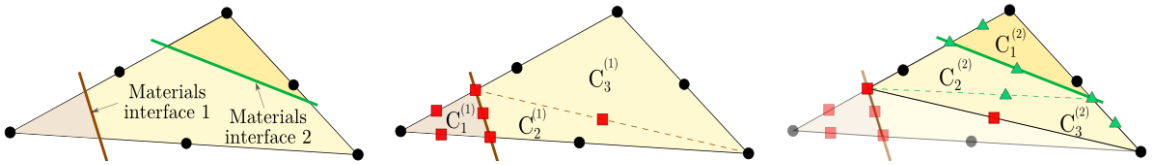

(a) (b) (c)

Figure 13. Hierarchical process of creating higher-order children elements for evaluating the enrichment function of a nonconforming six-node triangular element cut by two weak discontinuities: (a) configuration of interfaces; (b,c) children elements and enriched nodes at the first and second levels of hierarchy, respectively.

3.2.2) Enrichment for Strong Discontinuities (Cracks)

The HIFEM recursive algorithm can also accommodate higher-order polynomial enrichment functions along multiple strong discontinuities. A slightly different approach is used for the discretization of the children elements, though. Three new variations in the construction of the enrichment need to be implemented to the HIFEM algorithm.

First, elements intersected by cracks but not containing a crack tip are treated in a similar fashion as elements cut by weak discontinuities. The algorithm generates a set of triangular sub-domains whose boundaries align with the crack geometry. However, in

order to approximate the jump in the displacement field, the number of nodes (and thus, dofs) generated over crack interfaces will be double. Figure 14 shows the enrichment of two triangular elements intersected by straight cracks. In both cases, three additional nodes over the interface are required. Note that this configuration must be implemented to all 12 cases presented in the previous section (Figures 11 and 12).

Second, elements containing crack tips are also subdivided into a set of triangular elements whose boundaries align with the crack geometry. In this situation, only one enriched node is generated over the crack tip, and this node is being shared by all children elements created. As shown in Figure 15, 3 or 4 children elements are constructed from parent elements containing crack tips depending on whether the crack is intersecting a corner node.

Third, the critical $\sqrt{r}$ behavior of the displacement field given in equation (7) is incorporated by using *quarter-point crack tip isoparametric elements* developed in [35]. The singularity around crack tips is reproduced by moving non-corner midpoint nodes closer to the node located at the tip. The new location will be one quarter of the length of the corresponding edge from the tip as shown in Figure 15. Note that more quadrature points are needed for the integration of these elements.

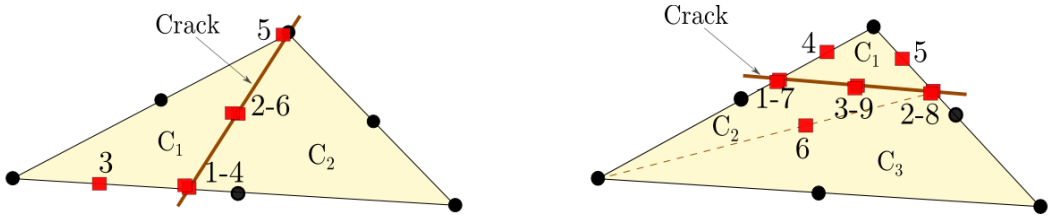

(a) (b)

Figure 14: Examples of configurations of enrichment for elements cut by cracks: in (a), a crack intersects an edge and a node, and thus only two children elements and 6 enriched nodes are generated. In (b), two edges are cut by the crack, resulting in three children elements and 9 enriched nodes. In both cases, 3 additional nodes are required over the material interface to simulate the strong discontinuity.

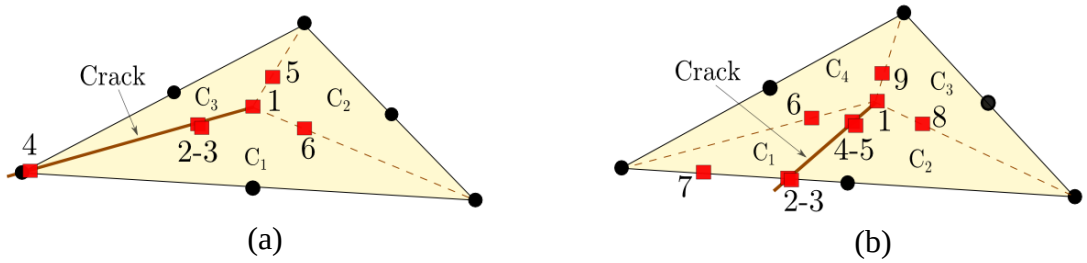

(a) (b)

Figure 15: Configurations of enrichment for elements containing a cracks tip. In (a) and (b) three and four children elements are constructed from a crack intersecting a corner node and an edge, respectively.

3.3) Higher-order HIFEM Implementation Issues.

Number of cases for the construction of children elements.

As mentioned before, the implementation of six-node triangular elements includes the creation of 12 cases for the construction of the children elements (see Figures 11 and 12). While the number of cases is not a major issue in the implementation of quadratic elements, defining individually all possible cases when dealing with higher-order polynomials of degree $p > 2$ can be problematic (e.g., 25 cases for cubic elements, 49 cases for quartic elements).

Scaling factor for higher-order HIFEM

While the proposed formulation for the scaling factor (see equation (13)) effectively stabilizes the conditioning of enrichment constructed by linear elements, this

is not always true when dealing with quadratic elements. The gradient of the shape functions for enriched nodes close to a midpoint node has a different behavior than for those close to a corner node. Thus, applying a scaling factor to quadratic enrichment ameliorates the conditioning of the stiffness matrix, but it does not stabilize it. It must be noted, however, that the accuracy of the results presented in next chapters are not compromised by the condition number of the global stiffness matrix since a direct solver was used for all the computations. Still, the conditioning of the linear systems computed for the example problems was monitored to verify that the approximations were not compromised by a high condition number.

Numerical integration for cracked domains.

A special numerical integration scheme is used for the computation of the enrichment of elements containing the crack tip to achieve more accurate approximations. We build a polar mapping of the integrand functions on a triangle from a quadrature rule on a square via a geometric transformation. In this configuration, more gauss points are located relatively close to the crack tip than in any ordinary quadrature rule on a triangle. This quadrature scheme, found in the literature as ‘almost polar integration’ or ‘singular mapping’, has been proof to perform better in other FEM-based techniques [36], [34]. The classical Gauss quadrature is kept on elements not containing crack tip nodes to avoid unnecessary computational cost.

Effectiveness of enrichment for crack tips.

While the configuration for the construction of enrichment for strong discontinuities described in the previous section is able to capture the discontinuous displacement field in a cracked domain, the accuracy of the HIFEM approximations is greatly dependent on the mesh employed. For example, consider two situations: (i) a crack tip is located at the centroid of an existing element, and (ii) a crack tip is in close proximity to the boundaries of the parent element. In (i), children elements are constructed with appropriate shapes and sizes, and are able to capture the high gradients close to the singularity. On the other hand, in (ii), children elements are unevenly distributed, which leads to a bad approximation of stress gradients. This issue is not mitigated by incorporating blending elements in a ring-shaped subdomain around the tip since in this approach only crack tip elements reproduce the singularity. Thus, the accuracy of the approximation on regions surrounding crack tips will rely upon the relative location of the tips with respect to the edges of the elements of all the levels of enrichment, regardless of the quadrature rule or blending strategy employed.

In an attempt to improve the level of precision in the approximations, several strategies to hierarchically accommodate higher-order polynomial enrichment functions in the vicinity of crack tips were investigated. The optimal strategy to circumvent the issue mentioned above is depicted in Figure 16. This approach generates a high number of degrees of freedom in regions surrounding crack tips after creating the children elements resulting from crack paths. *Pseudo-interfaces* are defined from the crack tip to

nodes of the nonconforming mesh in such way that a considerable number of enriched nodes are placed in all directions. The materials properties remain the same on both sides of the intersected elements, since the sole reason for adding these pseudo-interfaces is to generate more enriched nodes in the critical zones around crack tips.

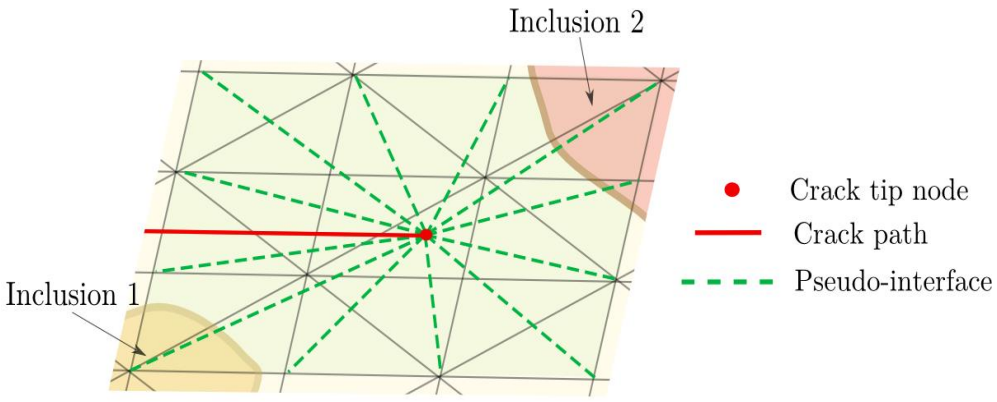

Figure 16: Strategy to improve the enrichment around crack tips. Pseudo interfaces are added sequentially to a small region containing a crack tip to increase the number of enriched nodes in its surroundings.

Two remarks need to be made for this approach. First, the enrichments for elements other than the parent crack tip element are constructed using the regular six-node triangular Lagrangian element. Blending elements are not considered since implementing them would require manipulation of enriched nodes. Moving these nodes closer to the tip to reproduce the singularity might be a daunting and inadequate task due to the varied distributions, sizes, and aspect ratios of elements surrounding the tips. Second, regardless of the sequence in which the pseudo-interfaces are added, a concentration of enriched nodes in a small region is inevitable. This uneven distribution

of enrichments results in configurations that are more sensible to the stress singularities on only a portion of the enriched region.

Chapter 4: Convergence Study

In this chapter, we investigate the accuracy and convergence of HIFEM with respect to standard FEM. We study the L_2- and H_1- norms of the error for the higher-order HIFEM benchmark problems simulations (a similar work for linear enrichment can be found in [28]). Two second-order HIFEM approximations with straight and curved material interfaces are presented in the following section. The first benchmark problem corresponds to a thermal problem with heat generation, and the second one models the stresses in a solid mechanics problem. To analyze the accuracy and convergence rate of this method, we study the variations of the L_2- and H_1-norms of the error defined as follows:

$$E_{L_2(\Omega)} = \sqrt{\int_\Omega \|u - u^h\|^2 d\Omega}$$
$$E_{H_1(\Omega)} = \sqrt{\int_\Omega (\|u - u^h\|^2 + \|\nabla u - \nabla u^h\|^2) d\Omega}. \quad (14)$$

As shown in the following benchmark problems, the higher-order HIFEM yields a similar precision and convergence rate as those of the standard FEM with respect to both norms of the error.

4.1) Benchmark Problems: Heat Conduction Example

In this first example problem, we study the performance of six-node triangular elements for the HIFEM simulation of the conductive heat conduction in an adhesive bonded joint (see Figure 17a for a full description of the problem). The thermal conductivities of the steel adherends and the adhesive layer are κ_{st} = 50.0 W/m K and κ_{st} = 1.00 W/m K, respectively. The boundary conditions consists of the prescribed temperatures $\bar{u}$ = 0 °C and $\bar{u}$ = 100 °C along the bottom and top edges of the domain, respectively, while the side edges are insulated. A linearly varying heat source of Q_{st} = $120y$ W/m^2 is also applied to the adherends (Q_{ad} = 0 W/m^2). The analytical solution for the temperature field in this problem is given by

$$\begin{array}{cc} T = -0.4y^3 + 43.83y & 0 \text{ cm} \leq y \leq 5.2 \text{ cm} \\ T = 568.9y - 2786.7 & 5.2 \text{ cm} \leq y \leq 5.3 \text{ cm} \\ T = -0.4y^3 + 45.09y + 49.14 & 5.3 \text{ cm} \leq y \leq 10 \text{ cm} \end{array} \quad (15)$$

The HIFEM approximation of the thermal response of this problem using a 16x8 structured mesh of six-node triangular elements is depicted in Figure 17b. The figure also illustrates the temperature profile in the *y*-direction, which clearly demonstrates the ability of the second-order HIFEM to capture gradient discontinuities in the temperature field.

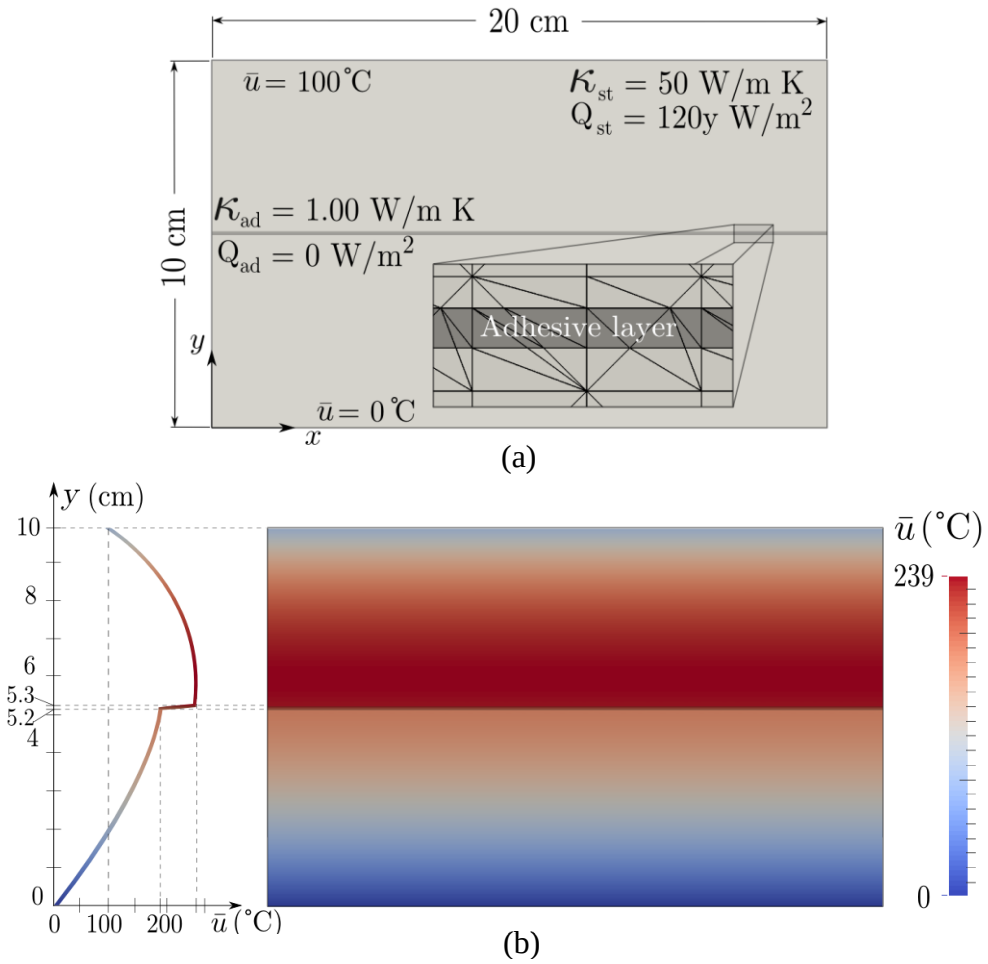

Figure 17. First convergence study problem: (a) domain geometry, material properties and boundary conditions for a system of two metallic sheets bonded by a thin adhesive layer. Additionally, the nonconforming and children elements belonging to the highest level of hierarchy are depicted in the inset. (b) HIFEM approximation of the temperature field using a 16x8 structured mesh of six-node triangular elements for discretizing the domain.

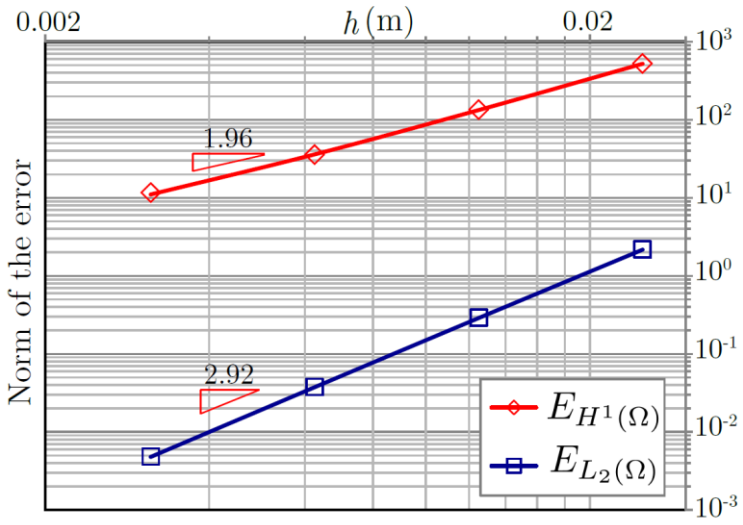

Figure 18. Convergence study for problem presented in Figure 17. Variations of the L_2- and H_1- norms of the error versus the element size (h) for the second-order HIFEM approximation.

Figure 18 provides the variations of the L_2- and H_1-norms of the error for the second-order HIFEM approximation of the temperature field versus the element size (h). For this benchmark problem, we use four nonconforming structured meshes of six-node triangular elements with resolutions 8x4, 16x8, 32x16, and 64x32 to discretize the domain. The middle row of elements in all these meshes is cut by both the upper and lower adhesive-adherend interfaces as depicted in Figure 17a. Under these conditions, higher-order HIFEM algorithm creates two levels of quadratic enrichment that yields optimal convergence rates with respect to both norms of the error, i.e., similar to those of the second-order standard FEM with conforming meshes ($E_{L_2(\Omega)}$ = 3, $E_{H^1(\Omega)}$ = 2).

4.2) Benchmark Problems: Solid Mechanics (Plane Stress) Example

In this example, we compare the accuracy and convergence rates of the second-order HIFEM with those of the standard FEM for simulating the deformation response of the plane stress problem shown in Figure 7a. The 100 μm x 100 μm domain consists of an aluminum matrix (E_{al} = 70 GPa, ν_{al} = 0.334) with embedded iron (E_{fe} = 200 GPa, ν_{fe} = 0.17) and silicon (E_{si} = 160 GPa, ν_{si} = 0:28) circular inclusions. A compressive uniform load of $\bar{f}$ = 50 kN/m is applied along the top edge while its bottom edge is constrained against horizontal and vertical displacements. Figure 19b illustrates the second-order HIFEM approximation of the normal stress field in the x-direction using an 80x80 structured mesh of six-node triangular elements for modeling the problem. Note that due to the close proximity of the embedded inclusions, several nonconforming elements are cut by two material interfaces in this simulation.

The Variations of the L_2- and H^1- norms of the error versus h for the second-order HIFEM and the standard FEM approximations of the deformation response of this second example problem are depicted in Figure 20. Five structured meshes of six-node triangular elements with resolutions 10x10, 20x20, 40x40, 80x80, and 160x160 are used to create discretized models for the HIFEM simulations. Conforming FE meshes with similar levels of refinement are used to discretize the domain in the standard FEM analyses, although creating finer elements in the vicinity of inclusions located close to one another is inevitable. Since there is no analytical solution to this problem, a second-order standard FEM approximation using a highly refined conforming FE mesh with max $(h) \approx 0.12$ μm (688,731 elements) is adopted as the reference solution for the error

analysis. As shown in Figure 20, the HIFEM yields a similar precision and convergence rate as those of the standard FEM with respect to both norms of the error for simulating this problem.

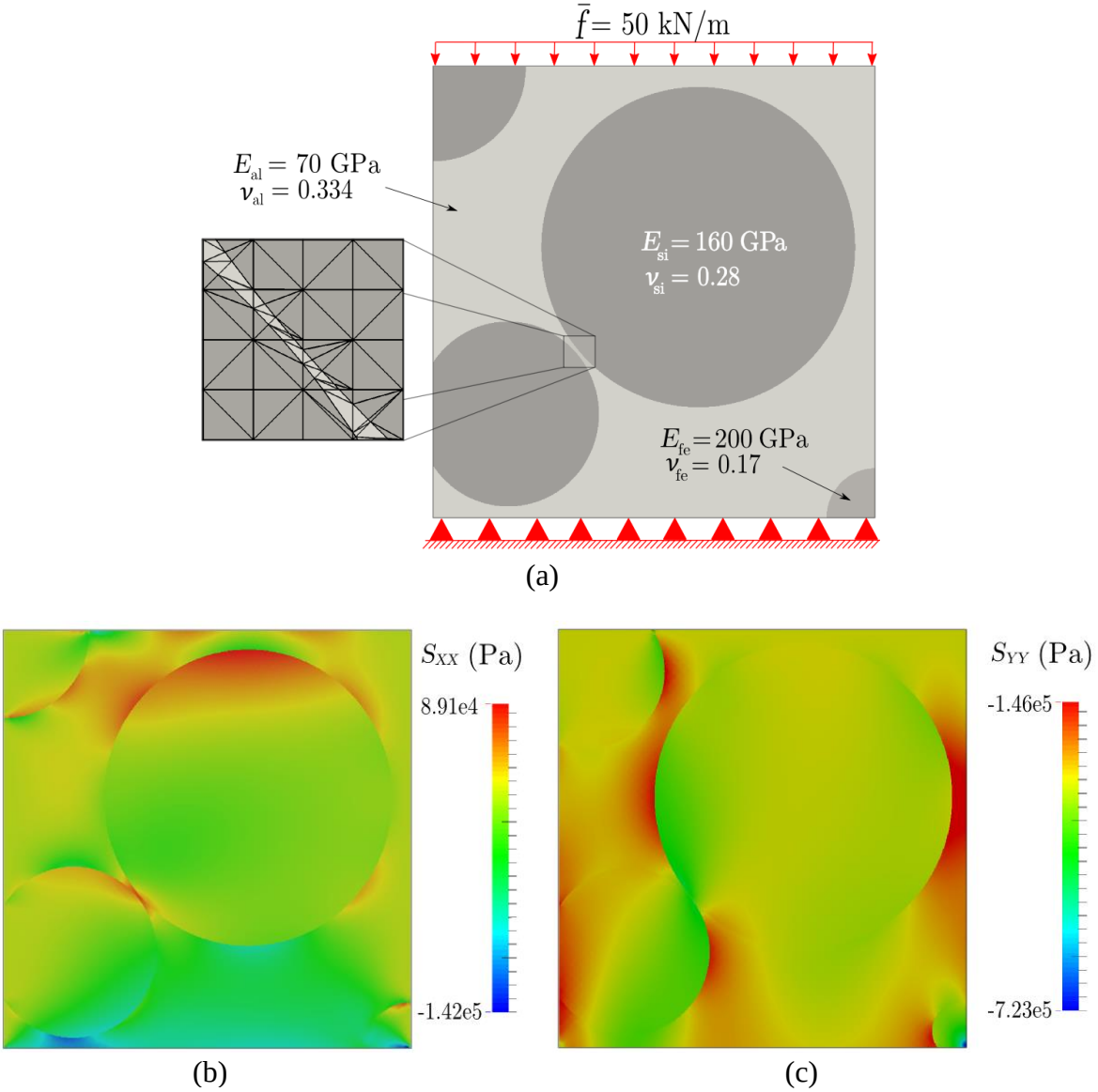

Figure 19. Second convergence study problem: (a) domain geometry, material properties, and boundary conditions; (b) and (c) second-order HIFEM approximation of the plane stress field in the x- and y- directions respectively, using an 80x80 structured mesh of six-node triangular elements for modeling the problem.

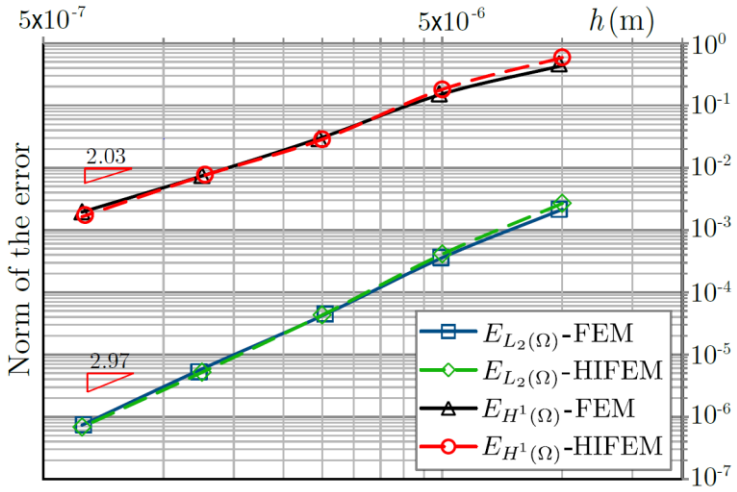

Figure 20. Comparison between the variations of the L_2- and H_1- norms of the error versus the element size (h) for the second-order HIFEM and standard FEM simulations of the deformation response of the second convergence study problem shown in Figure 19.

Chapter 5: Application Problems

In this chapter we demonstrate the application of the higher-order HIFEM for simulating the thermal and deformation responses of several engineering problems with complex morphologies. Higher-order elements are more appropriate for simulating the stress field in structural problems compared to linear triangular elements. For this reason, all the simulations are conducted using structured FE meshes composed of six-node triangular elements for discretizing the domain.

In the following application problems, the mesh-independent approach of the second-order HIFEM algorithm provides an easy-to-implement computational tool for the simulation of highly intricate morphologies. The HIFEM automated framework can easily handle Dirichlet boundary conditions along the side edges of this domain, and successfully capture sites of stress concentrations.

5.1) Application 1: Thermal and Mechanical Responses of a Porous Media

FE simulation of porous materials has been traditionally addressed using overly simplified microstructures. Issues associated with porous structures, such as overlapping interfaces, are frequently excluded or approximated to a simpler geometry. In our first application problem, we show the temperature and stress fields for a titanium matrix with pores arranged in a high level of complexity. In this example, the HIFEM algorithm evaluates the thermal response and the stress fields for two similar porous microstructures

of a titanium foam, as shown in Figures 21a and 22a, respectively. The titanium has a thermal conductivity of κ_{ti} = 21.9 W/m K, an elastic modulus of E_{ti} =110 GPa, and a Poisson ratio of ν_{ti} = 0:33. To construct HIFEM models of this porous microstructure, circular shape pores are hierarchically added to the 100x100 background structured FE mesh at arbitrary locations, resulting in pores that are located in close proximity and even overlapping with one another, as depicted in the insets of Figure 10a.

The boundary conditions of the thermal problem consists of the fixed temperature $\bar{u}$ =100 °C along the side edges, a constant heat flux of $\bar{q}$ = 170 W/m K along the bottom edge, and a convective upper boundary with the heat transfer coefficient $\bar{h}$ = 20 W/m K subjected to an ambient temperature of u_∞ = 21 °C (Figure 21a). The HIFEM approximation of the temperature field in this porous titanium composite is illustrated in Figure 21(b). Note that unlike XFEM/GFEM, the HIFEM can easily handle the Dirichlet boundary conditions along the side edges of this domain [23].

To simulate the mechanical behavior of the porous titanium microstructure shown in Figure 22(a), we assume the plane stress condition with a fixed displacement constraint along the bottom edge and constant applied tractions of $\bar{f}$ = 3.5 kN/m along the side edges of the domain. The deformed configuration and the HIFEM approximations of the x- direction normal stress and shear stress fields are depicted in Figures 22b and 22c, respectively. As shown in those figures, the second-order HIFEM can successfully capture sites of stress concentrations in this plane stress problem.

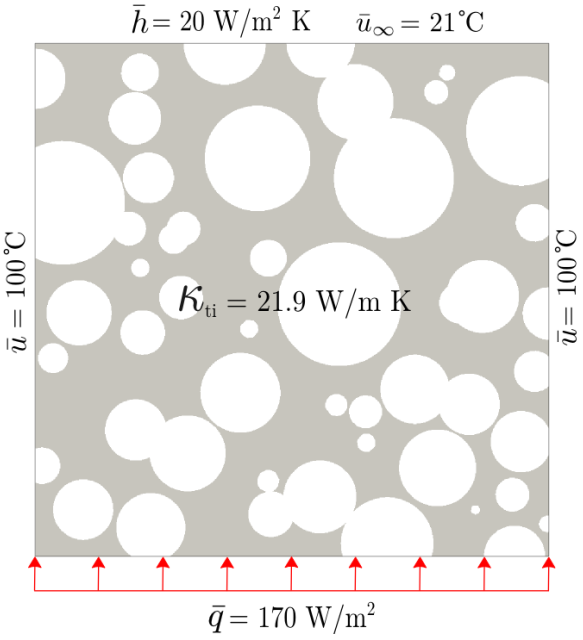

(a)

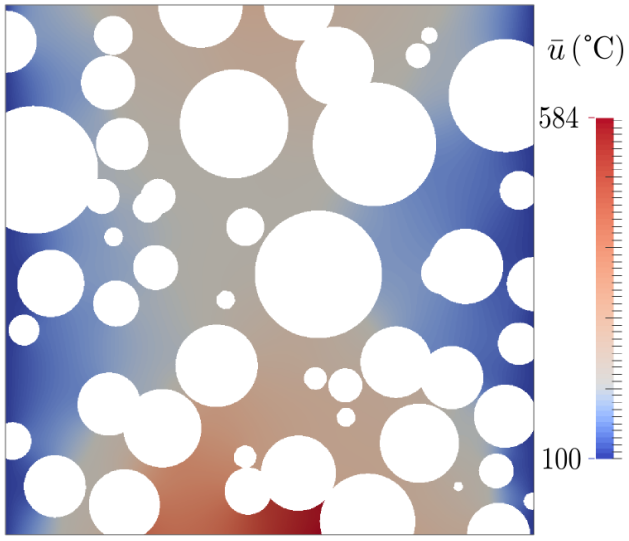

(b)

Figure 21. First application problem: (a) 4.5 mm x 4.5 mm porous titanium and boundary conditions of the thermal problems; (b) second-order HIFEM approximation of the temperature field.

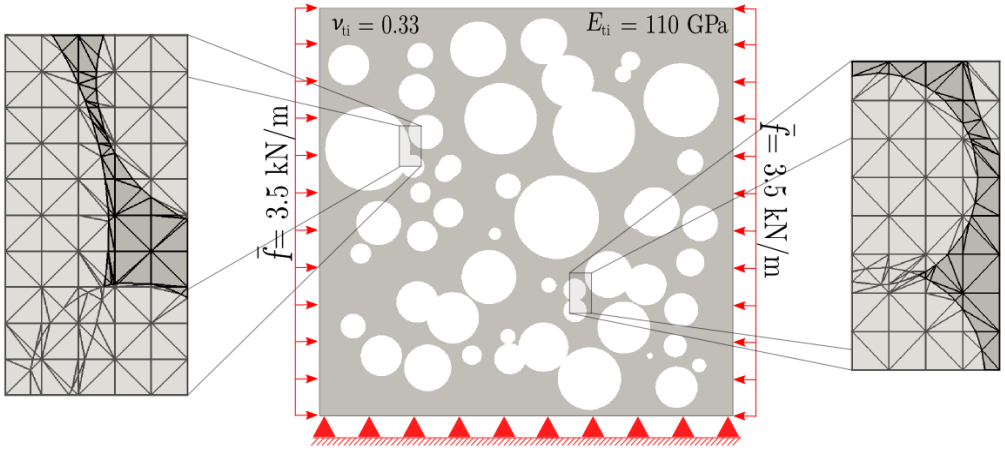

(a)

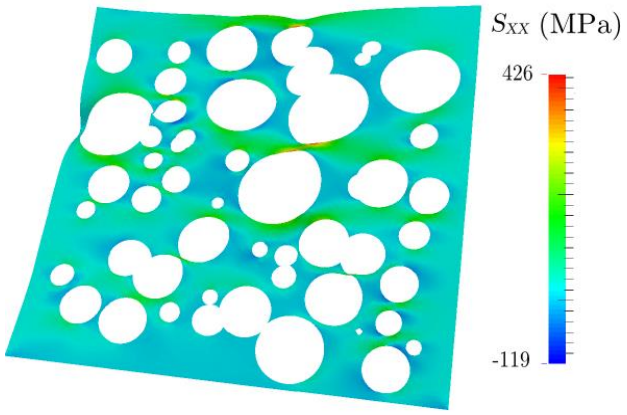

(b)

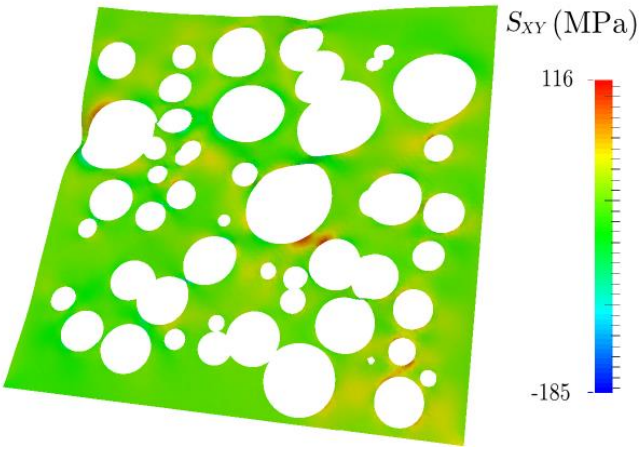

(c)

Figure 22. First application problem: (a) 5 mm x 5 mm porous titanium microstructure and boundary condition of the plane stress linear elasticity problem; (b,c) second-order HIFEM simulation of the normal and shear stresses, respectively.

5.2) Application 2: Pitting Corrosion Induced Stress Concentrations

Corrosion pits induce stress concentrations and thus serve as sites of crack nucleation, which can considerably accelerate the mechanical failure in structures such as aircrafts, bridges, and pipelines that are prone to the pitting corrosion phenomenon. Due to the complex evolving morphology of corrosion pits, creating conforming FE meshes to simulate the mechanical behavior of the corroded material with the standard FEM can be a challenging task. In contrast, the mesh-independent approach of the HIFEM provides an easy-to-implement computational tool for the treatment of this problem.

In this example problem, we demonstrate the application of the higher-order HIFEM for evaluating the stress field in a 20 cm x 5 cm axially loaded steel beam (E_{st} = 200 GPa, ν_{st} = 0.355) subjected to the pitting corrosion, as shown in Figure23(a). The simulated stress concentrations in the corroded beam of Figure 23(a) are illustrated in Figures 23(b) and 23(c), where a 360x90 structured FE mesh is implemented to discretize the bounding box of the domain. As shown in the insets of these figures, the HIFEM can easily capture the stress concentrations in the vicinity of interacting pits, i.e., in elements cut by two or more intersecting pit boundaries.

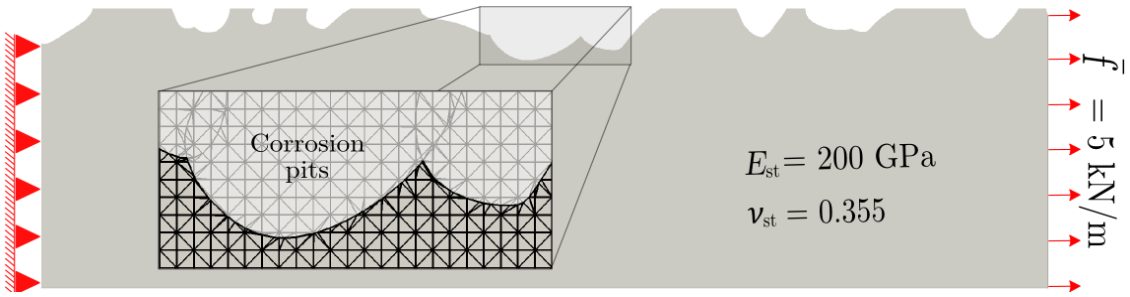

(a)

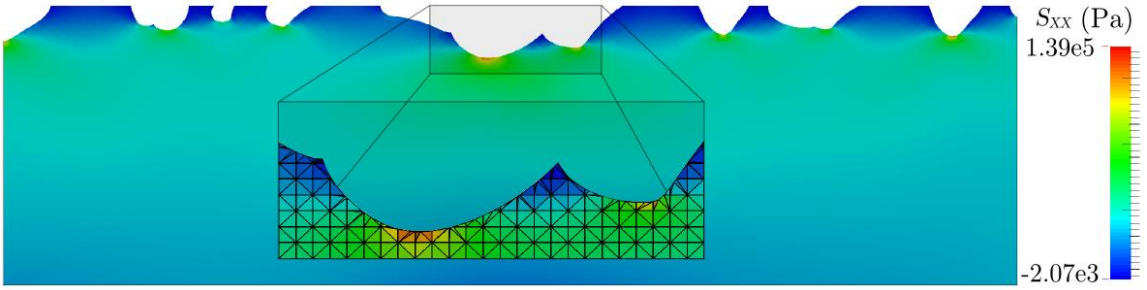

(b)

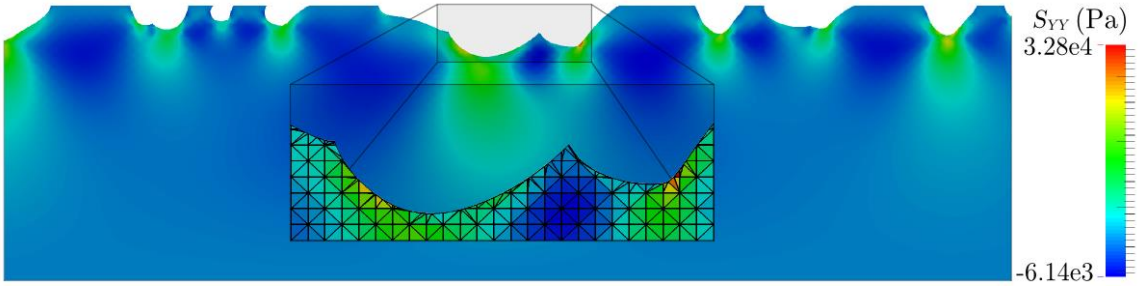

(c)

Figure 23. Second application problem: (a) 20 cm x 5 cm axially loaded steel beam subjected to pitting corrosion; (b,c) HIFEM approximation of normal stresses in the x- and y- directions.

5.3) Application 3: heterogeneous material mechanical behavior

In this example problem, we implement the HIFEM to simulate the mechanical behavior of a 4.5 μm x 4.5 μm composite with copper matrix and randomly oriented embedded carbon fibers (E_f = 300 GPa, E_m = 85 GPa, and ν_f = ν_m = 0.3), as shown in

Figure 24(a). The left edge of this heterogeneous material is constrained against horizontal and vertical displacements while a uniform distributed load of $\bar{f}$ = 30 N/m is applied along its right edge. Figures 24(b) and 24(c) illustrate the HIFEM approximation of the normal stress fields using a 100x100 structured FE mesh for discretizing the domain. Note that despite the intricate hetero-structure of this composite material system, the HIFEM provides the ability to simulate the stress concentrations along the fiber-matrix interfaces.

5.4) Application 4: Stationary Crack on a Heterogeneous Domain

In this final application example, we present the implementation of the HIFEM algorithm to linear elastic fracture mechanics problems. Figure 25 depicts two heterogeneous microstructures comprised of randomly distributed circular inclusions with a stationary crack. The two different 10 μm x 10 μm domains have the following material properties: E_{m} = 200 GPa, E_{in} = 300 GPa; ν_{m} = 0.33, ν_{in} = 0.25. The bottom edge of this heterogeneous material is constrained against horizontal and vertical displacements while a uniform distributed load of $\bar{f}$ = 50 N/m is applied along the top edge. As shown in both insets, the element containing the crack tip is further discretized in smaller children elements with the crack tip node common to all of them. In addition, the strong discontinuity is reproduced by a double number of dofs is introduced along the crack.

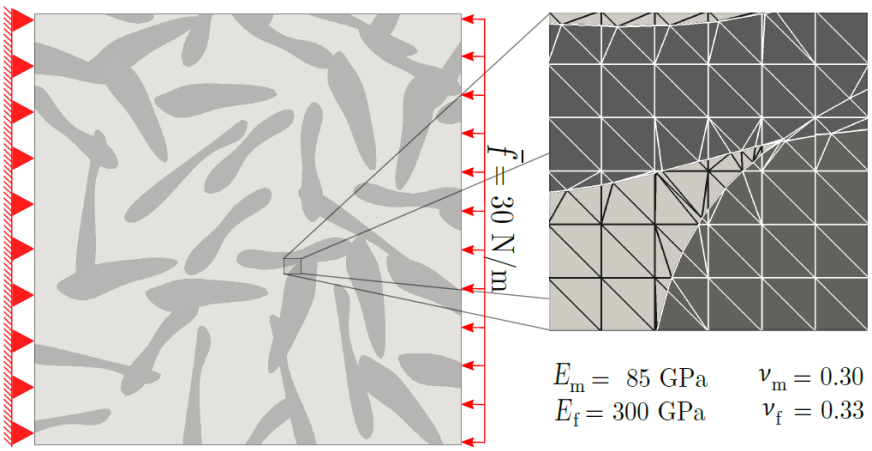

(a)

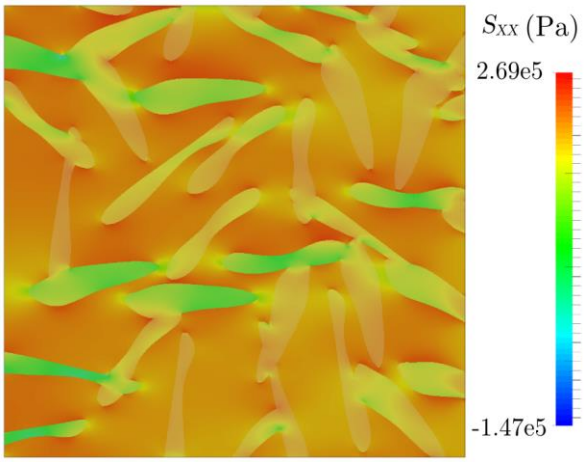

(b)

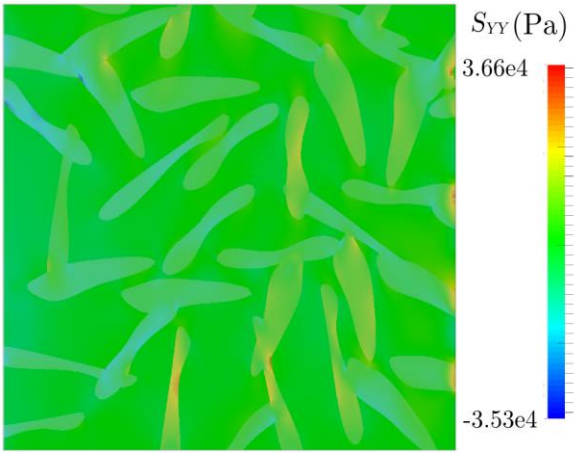

(c)

Figure 24. Third application problem: (a) 4.5 μm x 4.5 μm of a copper matrix carbon reinforced composite microstructure and boundary conditions; (b,c) HIFEM approximation of normal stresses using a 100x100 structured FE mesh for discretizing the domain.

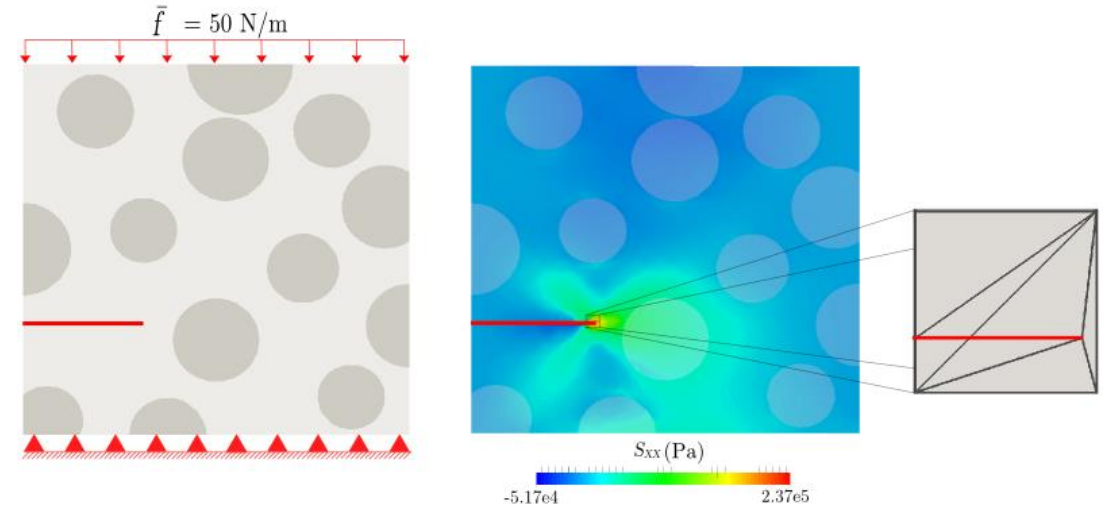

(a)

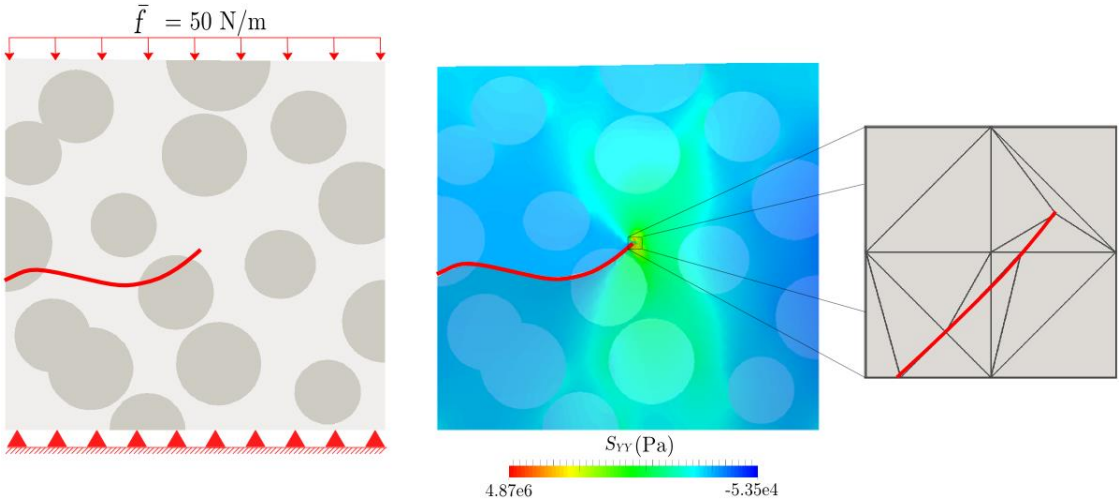

(b)

Figure 25. Fourth application problem: Simulation of two cracked heterogeneous domains using 51x51 structured FE meshes. (a, b) Normal stress distributions in the x- and y- directions with mesh insets for a straight and a curved crack, respectively.

Chapter 6: Conclusions and Future Work

6.1) Conclusions

This thesis describes the development of a mesh-independent FEM technique that eases the laborious and time-consuming process of modeling problems with complex and/or evolving morphologies by automatically introducing hierarchical enrichment in regions surrounding the discontinuities. The algorithm for a hierarchical interface-enriched finite element method (HIFEM) was improved to include the evaluation of enrichment functions of higher-order Lagrangian elements. While the focus of this thesis is the implementation of six-node triangular elements and its applications, the proposed approach is general and can be expanded to other types of higher-order Lagrangian elements. The higher-order HIFEM algorithm relies on the hierarchical construction of distorted children elements in nonconforming elements cut by multiple material interfaces for the numerical approximations of domains with weak discontinuities. A special mapping that maintains a constant Jacobian was introduced to evaluate distorted children elements in the local coordinates system. This approach minimizes the computational cost and obviates the difficulties associated with the construction of distorted integration elements.

For the simulation of cracked domains, additional enriched nodes are added along crack paths to reproduce the strong discontinuity, and triangular quarter point elements are constructed around crack tips to reproduce the singularity of the stress fields.

Furthermore, pseudo-interfaces are hierarchically introduced to a small region around the tips to increase the number of enriched nodes and achieve a more accurate approximation.

A convergence study was performed to show that the second order HIFEM yields a similar precision and convergence rate as those of the standard FEM with conforming meshes of quadratic triangular elements. The higher-order HIFEM was also applied in the mesh-independent modeling of the thermal and structural responses of varying engineering problems with complex weak and strong discontinuities. Example of realistic simulations using the proposed method, including a porous titanium composite, a cantilever beam subjected to pitting corrosion, a heterogeneous metal matrix composite, and a stationary crack were also presented.

6.2) Future Work

Geometrical representation of the discontinuities

The Lubachevsky-Stillinger algorithm (LS algorithm) can be employed to generate virtual microstructures modeled with the HIFEM (see Appendix A). To improve the geometrical representation of weak and strong discontinuities, the LS algorithm can be combined with Non-Uniform Rational B-Splines (NURBS). Besides describing a more realistic geometry, NURBS would allow the HIFEM to directly import CAD drawings, which can significantly automate the process of incorporating embedded particles, as well as voids, in microscopic models.

Hybrid approaches for crack simulations

Numerical techniques, such as the Level Set Method (LSM), could be incorporated into the HIFEM algorithm to ease the handling of evolving complex geometries in heterogeneous domains. In addition, other mesh-independent techniques, such as the extended finite element method (XFEM) could be integrated with the HIFEM to achieve improved precision and efficiency for certain problems. In a "hybrid XFEM/HIFEM" approach, the HIFEM enrichment could still be used to capture weak discontinuities (e.g., inclusions and voids) and part of strong discontinuities (e.g., crack paths). The XFEM enrichment could be blended with the HIFEM enrichments at the first level of hierarchy to provide an accurate approximation of stress concentrations in regions surrounding crack tips. This hybrid approach would be attractive to analyze the perturbation of the local stress field near crack tips and the behavior of cracks propagating quasi-statically in complex microstructures.

Optimization problems

The HIFEM is an appropriate method for the computational design of material microstructure to achieve improved performance. Its recursive algorithm can easily automate the modeling process of discrete optimization problems to match desired material properties with the integration of numerical tools, such as the genetic algorithm (GA). An example of this could be the virtual characterization and optimization of functionally graded composite microstructures.

References

[1]. P. Frey and P. L. George. Mesh Generation. John Wiley & Sons, 2010.

[2]. M. Beall, J. Walsh, and M. Shephard. Accessing cad geometry for mesh generation. In IMR, pages 33–42, 2003.

[3]. A. Reid, S. Langer, R. Lua, V. Coffman, S. Haan, and R. García. Image-based finite element mesh construction for material microstructures. Computational Materials Science, 43(4):989–999, 2008.

[4]. P.M. Cattaneo, M. Dalstra, and L.H. Frich. A three-dimensional finite element model from computed tomography data: a semi-automated method. Proceedings of the Institution of Mechanical Engineers, Part H: Journal of Engineering in Medicine, 215(2):203–212, 2001.

[5]. J.C. Cuillière, V. Francois, and J.M. Drouet. Automatic mesh generation and transformation for topology optimization methods. Computer-Aided Design, 45(12):1489–1506, December 2013.

[6]. R. Kannan, S. Hendry, N. Higham, and F. Tisseur. Detecting the causes of ill-conditioning in structural finite element models. Computers & Structures, 133:79–89, 2014.

[7]. R. Guldberg, S.J. Hollister, and G.T. Charras. The accuracy of digital image-based finite element models. Journal of Biomechanical Engineering, 120(2):289–295, 1998.

[8]. Q. Lu, M. S. Shephard, S. Tendulkar, and M. W. Beall. Parallel mesh adaptation for high-order finite element methods with curved element geometry. Engineering with Computers, 30(2):271–286, 2014.

[9]. X. Y. Zhu, W. Q. Chen, Z. Y. Huang, and Y. J. Liu. Fast multipole boundary element analysis of 2D viscoelastic composites with imperfect interfaces. Science China Technological Sciences, 53(8):2160–2171, 2010.

[10]. Y. J. Liu, S. Mukherjee, N. Nishimura, M. Schanz, W. Ye, A. Sutradhar, E. Pan, N. A. Dumont, A. Frangi, and A. Saez. Recent advances and emerging applications of the boundary element method. Applied Mechanics Reviews, 64(3):1001, 2011.

[11]. H. T. Wang and Z. H. Yao. Large-scale thermal analysis of fiber composites using a line-inclusion model by the fast boundary element method. Engineering Analysis with Boundary Elements, 37(2):319–326, 2013.

[12]. T. Belytschko, Y. Krongauz, D. Organ, M. Fleming, and P. Krysl. Meshless methods: an overview and recent developments. Computer methods in applied mechanics and engineering, 139(1):3–47, 1996.

[13]. B Movahedian, B Boroomand, and S Soghrati. A trefftz method in space and time using exponential basis functions: application to direct and inverse heat conduction problems. Engineering Analysis with Boundary Elements, 37(5):868–883, 2013.

[14]. A. Rosolen, C. Peco, and M. Arroyo. An adaptive meshfree method for phase-field models of biomembranes. Part I: approximation with maximum-entropy approximants. Journal of Computational Physics, 249:303–319, 2013.

[15]. Soheil Soghrati, Weijie Mai, Bowen Liang, and Rudolph G. Buchheit. A boundary collocation meshfree method for the treatment of poisson problems with complex morphologies. Journal of Computational Physics, 281:225–236, 2015.

[16]. L. Zhang, A. Gerstenberger, X. Wang, and W. K. Liu. Immersed finite element method. Computer Methods in Applied Mechanics and Engineering, 193(21-22):2051–2067, 2004.

[17]. C. T. Wu, Y. Guo, and E. Askari. Numerical modeling of composite solids using an immersed meshfree galerkin method. Composites Part B: Engineering, 45(1):1397–1413, 2013.

[18]. S. Kumar, I. V. Singh, and B. K. Mishra. A multigrid coupled (FE-EFG) approach to simulate fatigue crack growth in heterogeneous materials. Theoretical and Applied Fracture Mechanics, 2014.

[19]. T. J. Oden, C. A. Duarte, and O. C. Zienkiewicz. A new cloud-based hp finite element method. Computer Methods in Applied Mechanics and Engineering, 153(1-2):117–126, 1998.

[20]. Babuska and J. M. Melnek. The partition of unity method. International Journal for Numerical Methods in Engineering, 40(4):727–758, 1997.

[21]. V. Singh, B. K. Mishra, M. Brahmankar, V. Bhasin, K. Sharma, and I. A. Khan. Numerical simulations of 3-d cracks using coupled EFGM and FEM. International Journal for Computational Methods in Engineering Science and Mechanics, 15(3):227–231, 2014.

[22]. T. Belytschko, R. Gracie, and G. Ventura. A review of extended/generalized finite element methods for material modeling. Modeling and Simulation in Material Science and Engineering, 17:043001, 2009.

[23]. S. Soghrati, A. M. Aragón, C. A. Duarte, and P. H. Geubelle. An interface-enriched generalized finite element method for problems with discontinuous gradient fields. International Journal for Numerical Methods in Engineering, 89(8):991–1008, 2012.

[24]. S. Soghrati and P. H. Geubelle. A 3D interface-enriched generalized finite element method for weakly discontinuous problems with complex internal geometries. Computer Methods in Applied Mechanics and Engineering, 217-220:46–57, 2012.

[25]. S. Soghrati, P. R. Thakre, S. R. White, N. R. Sottos, and P. H. Geubelle. Computational modeling and design of actively-cooled microvascular materials. International Journal for Heat and Mass Transfer, 2012.

[26]. S. Soghrati, A. R. Najafi, J. H. Lin, K. M. Hughes, S. R. White, N. R. Sottos, and P. H. Geubelle. Computational analysis of actively-cooled 3D woven microvascular composites using a stabilized interface-enriched generalized finite element method. International Journal of Heat and Mass Transfer, 65:153–164, 2013.

[27]. A. M. Aragón, S. Soghrati, and P. H. Geubelle. Effect of in-plane deformation on the cohesive failure of heterogeneous adhesives. Journal of Mechanics and Physics of Solids, 61:1600–1611, 2013.

[28]. S. Soghrati. Hierarchical interface-enriched finite element method: An automated technique for mesh-independent simulations. Journal of Computational Physics, 2014.

[29]. O. C. Zienkiewicz, R. L. Taylor, and J. Z. Zhu. The finite element method: its basis and fundamentals. Elsevier, 2005.

[30]. N. S. Lee and K. J. Bathe. Effects of element distortions on the performance of isoparametric elements. Int. J. Numer. Meth. Engng., 36(20):3553–3576, 1993.

[31]. H. G. Garnir. Singularities in Boundary Value Problems. Springer Science & Business Media, 1981.

[32]. T. Strouboulis, I. Babuka, and K. Copps. The design and analysis of the generalized finite element method. Computer Methods in Applied Mechanics and Engineering, 181(13):43–69, 2000.

[33]. Alexander Menk and Stphane P. A. Bordas. A robust preconditioning technique for the extended finite element method. International Journal for Numerical Methods in Engineering, 85(13):1609–1632, 2011.

[34]. E. Béchet, H. Minnebo, N. Mos, and B. Burgardt. Improved implementation and robustness study of the x-FEM for stress analysis around cracks. International Journal for Numerical Methods in Engineering, 64(8):1033–1056, 2005.

[35]. Roshdy S. Barsoum. On the use of isoparametric finite elements in linear fracture mechanics. International Journal for Numerical Methods in Engineering, 10(1):25–37, 1976.

[36]. Patrick Laborde, Julien Pommier, Yves Renard, and Michel Salan. High-order extended finite element method for cracked domains. International Journal for Numerical Methods in Engineering, 64(3):354–381, 2005.

Appendix A: Programs Assisting the HIFEM Code.

2D Mesh Generator

The graphical user interface (GUI) presented in Figure 27 creates '.inp' files, which are required as input to run the HIFEM Matlab code. This program generates structured nonconforming triangular meshes for two-dimensional problems following the Abaqus standard format (See Figure 26b). The user needs to define the dimensions of the domain and grid number in x and y direction, as well as the nature of the problem (heat conduction or structural) with the respective material properties and boundary conditions. While the configurations for the boundary conditions are restricted to simple Neumann and Dirichlet prescribed constant values, the HIFEM code has the capability to redefine such values to more complex, but realistic conditions.

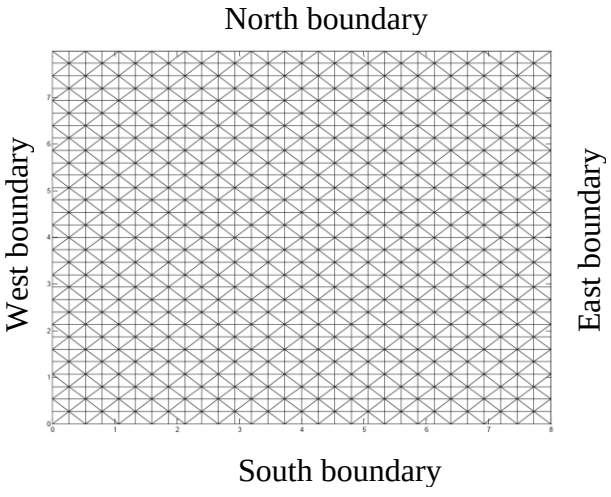

(a)

```
*HEADING
**ABAQUS input file created at 1-16-2015, 18:43:38
*NODE
1,     0.000000,       0.000000
2,     0.500000,       0.000000
3,     1.000000,       0.000000
4,     0.000000,       0.500000
5,     0.500000,       0.500000
6,     1.000000,       0.500000
7,     0.000000,       1.000000
8,     0.500000,       1.000000
9,     1.000000,       1.000000
**
**
*ELEMENT, TYPE=CPS6, ELSET=SOLID_MAT
1,    9,    7,    1,    8,    4,    5
2,    1,    3,    9,    2,    6,    5
**
**
**solid section
*SOLID SECTION, ELSET=SOLID_MAT,MATERIAL=asdf
1.,
**
**Material Properties
**
*MATERIAL, NAME=asdf
**
*DENSITY
321
**
*ELASTIC,TYPE=ISO
200e9,3.000000e-01
```

(b)

Figure 26. (a) Example of a structured nonconforming mesh representing a rectangular domain, and (b) example of an input file generated by the GUI shown in Figure 27.

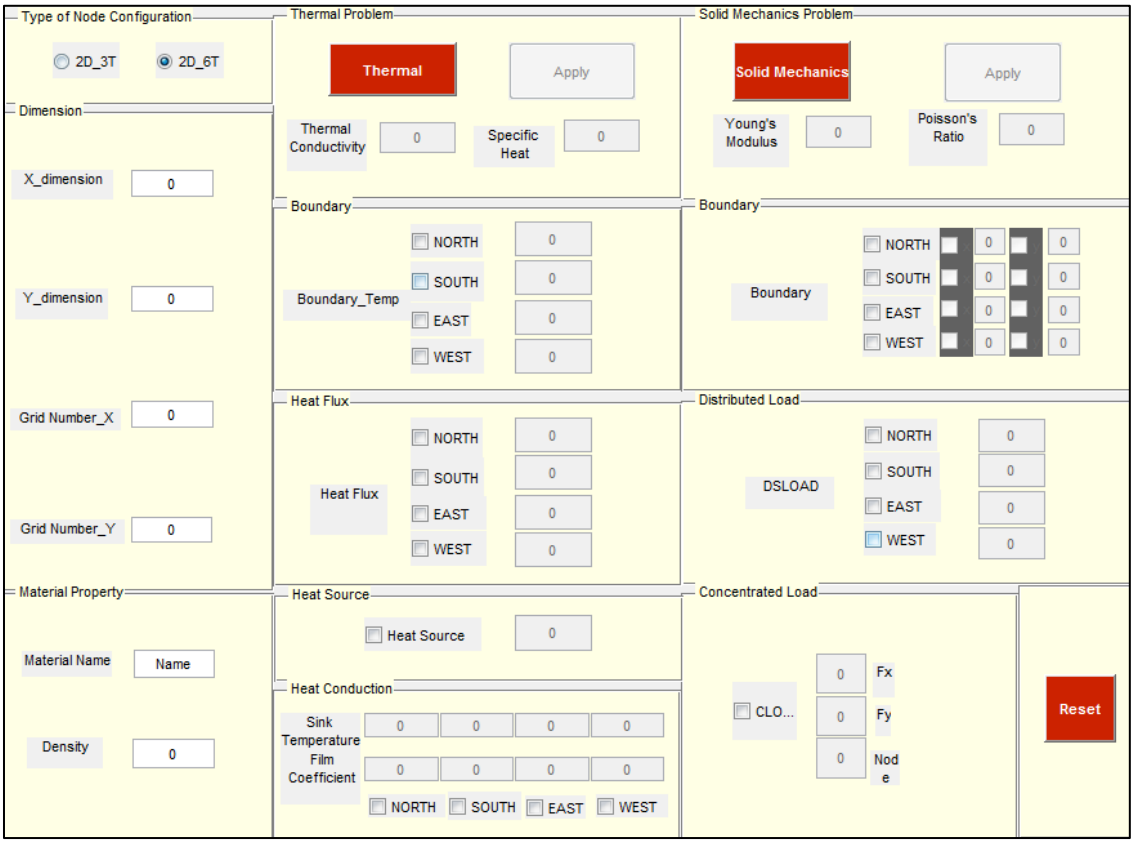

Figure 27. Matlab GUI to generate input files for the HIFEM code for thermal and structural problems using either linear (three-node) or quadratic (six-node) triangular elements.

Ellipsoidal inclusions generator

To generate random closely packed inclusions in a base material matrix we use an algorithm called Lubachevsky-Stillinger algorithm (LS algorithm) that simulates the process of compressing an assembly of particles as shown in Figure 28. The information used includes the coordinates of the center of each shape, and their corresponding radius.

No additional information is required if the geometry of the problem consists of only circular and/or ellipsoidal inclusions.

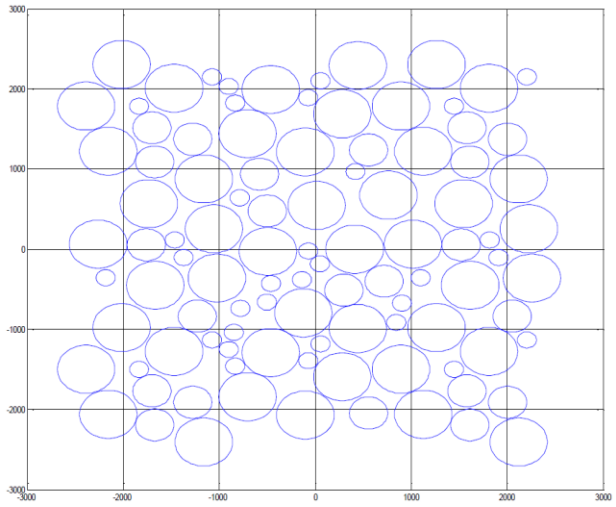

Fig. 28. Example of closely packed circles generated from the LS algorithm.

Inclusions geometry generator

For more realistic geometrical features, a set of arbitrary shape inclusions can be obtained from a scanning electron microscope (SEM) image of actual composite material. To accomplish this, a number of boundary points coordinate are identified for each inclusion in the figure. Then, using these data, the boundary curves are interpolated and normalized so the center is the origin and then each inclusion. Finally, the resulting vectors containing the geometry of the inclusions are combined with the coordinates and scale obtained from the LS algorithm to distribute them randomly in a given domain. Note that any given inclusions geometrical configuration (ellipsoidal or from SEM image) input to the HIFEM code can be manipulated in terms of size, volume fraction and/or number of particles.

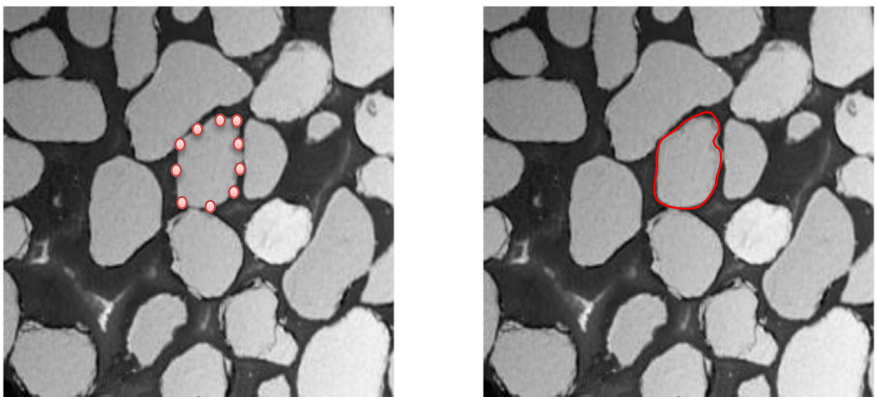

(a) (b)

Fig. 29. SEM image of composite material. (a) Control points are taken around the boundary of each inclusion, and (b) the geometry resulting from the control points.